MOST Status	Completion Date	Observing Frequency Range (MHz)	Instantaneous bandwidth (MHz)	Line feed Polarisation	Spectral Channels	Overall Sensitivity (12 hr 1σ/beam)	System Temp (K)	Independent Baselines	Infrastructure
MOST	1981	843	3	RH single circular	-	1–2 mJy	55	64	-
SKAMP 1	2006	843	3	RH single circular	-	0.8 mJy	55	4096	Continuum correlator.
SKAMP 2	2008	830–860	30	RH single circular	6000	0.2 mJy	55	4096	Spectral line correlator, polyphase filterbanks, new LO and optical fibre signal path.
SKAMP 3	2009	300–1400	100	Dual linear	6000	0.1 mJy	40	4096	New RF front-end architecture and mesh.

Table 3.1 Comparison of the three SKAMP stages with the existing MOST operation.

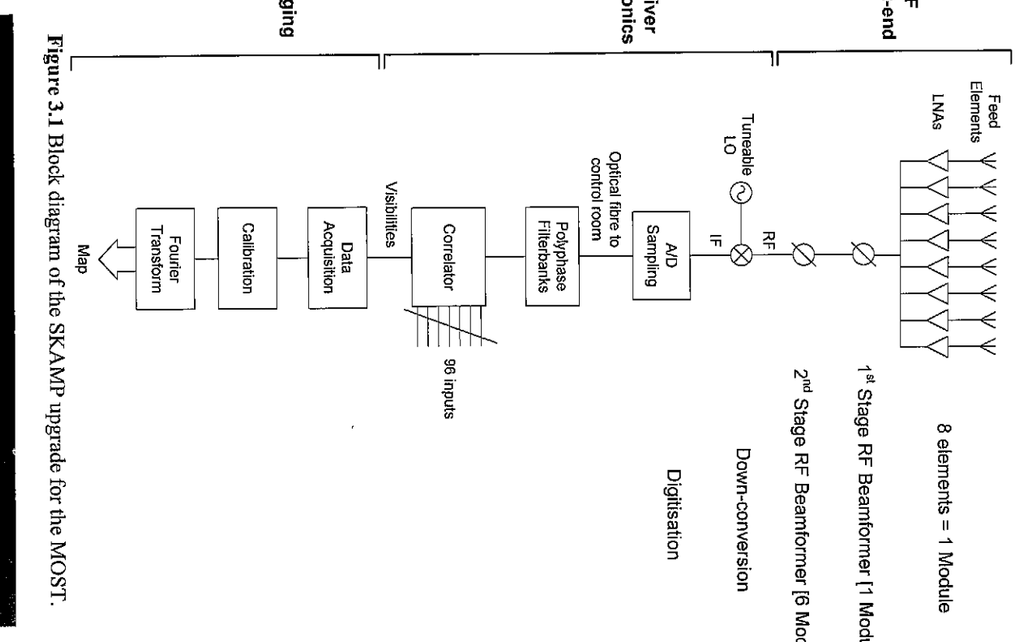

Figure 3.1 Block diagram of the SKAMP upgrade for the MOST.

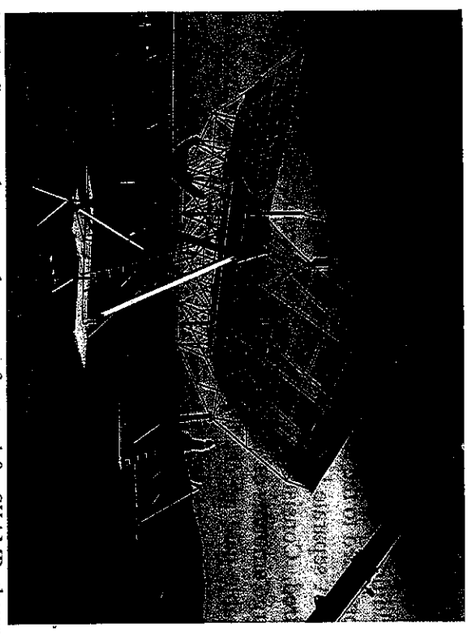

Figure 3.2 Cylindrical reflector test bay to evaluate new front-end for SKAMP, shown with the MOST behind. (D.Campbell-Wilson).

3.2 Key Enabling Technologies

Key components necessary for the SKAMP upgrade, presented in Section 3.1, are the line feed, electronics and infrastructure. The technologies that enable the implementation of these components are described next.

3.2.1 Line Feed

The existing circular ring line feed element (Mills and Little 1972) is retained for SKAMP 1 and 2. SKAMP 3 requires a feed that can sense two simultaneous polarisations over a wide frequency range. Scanning line feeds have been used in existing cylindrical reflector radio telescopes as listed in Table 1.2. However, these arrays operate with a narrow bandwidth and single polarisation. Currently no dual polarised wideband line feeds have been developed for cylindrical reflectors in radio astronomy. A dual polarised line feed has been developed for cylindrical reflector radar, described in Section 1.1.1, but its operating bandwidth is narrow and it is designed for an offset-fed reflector. Feed development for military, satellite and wireless communications applications has resulted in phased array elements having dual polarisation and wideband characteristics (Chio and Schaubert 1999; Lee et al. 2003; Ghorbani and Waterhouse 2004). An investigation into the current state-of-the-art phased array element technology and its suitability for the SKAMP line feed is presented in Chapter 4.

3.2.2 Electronics

Cost effective electronics are critical for the implementation of SKAMP. Since the 1960s, the cost of electronics has been reducing rapidly. Widespread use of RF CMOS technology in wireless communications receivers, offers the possibility of implementing an entire receiver on a single chip, called system-on-a-chip (SoC). Advantages of a SoC design are low manufacturing costs, integration of sub components, reduction of parasitics, size and power. For SKAMP, SoC can be used to integrate the receiver electronics after the RF beamformer and could include the tuneable LO, mixer, samplers, digitisers and additional IF amplifiers and filters. Because the first-stage LNA, shown in Figure 3.1, is connected to the beamformer before the down-conversion, it cannot be part of the main SoC. A separate LNA CMOS design such as the one described in Belostotski (2006) is required. Consistent advances in electronic technology have enabled the processing of large amounts of data using high speed, low cost electronic chips known as field programmable gate arrays (FPGA). This is the key technology for the SKAMP correlator design.

3.2.3 Infrastructure

Handling the correlator data rates requires a new optical IF digital distribution network. Consumer demand for broadband internet has led to the growth in technology required to implement these networks, including affordable low loss multimode optical fibre, high

speed optical routers and switches, wavelength division multiplexing and high capacity gigabit optical-electronic transceivers. Other infrastructure required for the SKAMP upgrade is the re-meshing of the reflector to reduce the system noise temperature at the upper frequency limit, as described in Section 3.1. The new mesh will be overlayed on top of the existing mesh. An efficient technique has been developed for attaching the new mesh (D. Campbell-Wilson, personal communication, 2005).

3.3 Line feed Engineering Parameters

This Section investigates the parameters used to evaluate the line feed performance for the SKAMP upgrade and their influence on telescope imaging. From this investigation, a set of design specifications is established to determine the design of a new line feed element. Because the MOST uses electronic and mechanical beam steering for aperture synthesis imaging, the performance of the line feed parameters is analysed subject to these operating conditions in both longitudinal and transverse planes.

3.3.1 Antenna Effective Area

The effective area, A_{eff}, describes the amount of aperture area that an antenna utilises for a particular application. For the MOST, this refers to the collecting area utilised for imaging. It has a direct relationship with the system sensitivity, shown in Equation 2.2 and designing the line feed to maximise the effective area improves the system sensitivity. A parameter that relates feed performance to effective area is the aperture efficiency, η_{ap}:

$$\eta_{ap} = \frac{A_{eff}}{A_p} \tag{3.1}$$

Where A_{eff} = effective area of the antenna aperture.

A_p = physical area of the antenna aperture.

For a reflector antenna, the aperture efficiency is the product of several sub-efficiency parameters that represent the total performance of the feed in a reflector:

$$\eta_{ap} = \eta_t \eta_{sp} \eta_{blk} \eta_{pol} \tag{3.2}$$

Where η_t = feed taper efficiency

η_{sp} = spillover efficiency

η_{blk} = blockage efficiency

η_{pol} = polarisation efficiency

As the MOST has a rectangular aperture, these sub-efficiencies are different for the longitudinal and transverse planes and are described separately.

Transverse plane

The MOST consists of a curved reflector and line feed cross section, with the line feed pattern illuminating the reflector as shown in Figure 3.3. The line feed pattern comprises co-polar, G_{cp}, and cross-polar, G_{xp}, (components) patterns, which are described in Section 3.3.4.

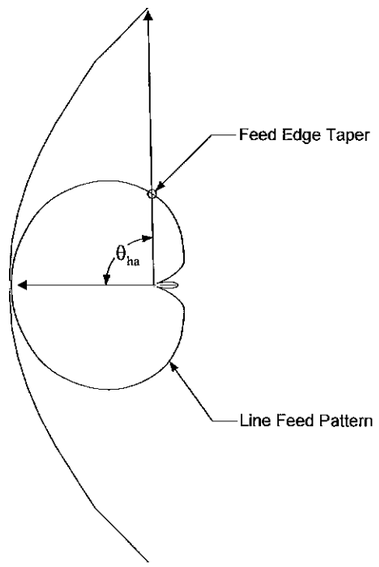

Figure 3.3 Line feed pattern illuminating the reflector in the transverse plane, showing the feed edge taper.

The feed taper efficiency, η_t represents the percentage of feed radiation captured by the reflector aperture compared to a uniform aperture illumination. This percentage is calculated for a known co-polar feed pattern G_{cp} and reflector geometry f/D. The taper efficiency for a parabolic reflector antenna is given by (Stutzman and Thiele 1998):

$$\eta_t = \frac{4f^2}{\pi a^2} \frac{\left[\int_0^{2\pi}\int_{-\theta_{ha}}^{\theta_{ha}} G_{cp}(\theta,\phi)\left|\tan\left(\frac{\theta}{2}\right)\right| d\theta d\phi\right]^2}{\int_0^{2\pi}\int_{-\theta_{ha}}^{\theta_{ha}} \left|G_{cp}(\theta,\phi)\right|^2 \left|\sin\theta\right| d\theta d\phi} \tag{3.3}$$

Where θ = pointing angle in the transverse plane

θ_{ha} = subtended half angle of the reflector

G_{cp} = co-polar feed gain

a = aperture radius ($D/2$)

f = focal length

Equation 3.3 can be adapted to suit a cylindrical reflector geometry, in the transverse plane, so the taper efficiency only depends on θ. This is done by substituting the identity

for the aperture radius: $a = 2f\tan(\theta_{ha}/2)$ into Equation 3.3 and assuming a constant ϕ, which gives:

$$\eta_t = 2\cot^2\left(\frac{\theta_{ha}}{2}\right) \frac{\left[\int_{-\theta_{ha}}^{\theta_{ha}} G_{cp}(\theta)\left|\tan\left(\frac{\theta}{2}\right)\right| d\theta\right]^2}{\int_{-\theta_{ha}}^{\theta_{ha}} \left|G_{cp}(\theta)\right|^2 \left|\sin\theta\right| d\theta} \tag{3.4}$$

Another parameter used to describe the reflector aperture illumination for a particular feed is called the feed edge taper and shown in Figure 3.3. This parameter describes the level of gain in the feed pattern at the angle corresponding to the reflector edge, θ_{ha}, compared to its peak.

When a feed illuminates a reflector, radiation not collected by the reflector is known as spillover, depicted by the hatched region in Figure 3.4. Spillover efficiency, η_{sp}, is the percentage of feed power collected by the reflector divided by the radiated feed power in all angular directions calculated for an antenna pointing at zenith by (Kildal 1984a):

$$\eta_{sp} = \frac{\int_{-\theta_{ha}}^{\theta_{ha}} \left[\left|G_{cp}(\theta)\right|^2 + \left|G_{xp}(\theta)\right|^2\right] d\theta}{\int_{-\pi}^{\pi} \left[\left|G_{cp}(\theta)\right|^2 + \left|G_{xp}(\theta)\right|^2\right] d\theta} \tag{3.5}$$

Where G_{cp} = co-polar gain

G_{xp} = cross-polar gain

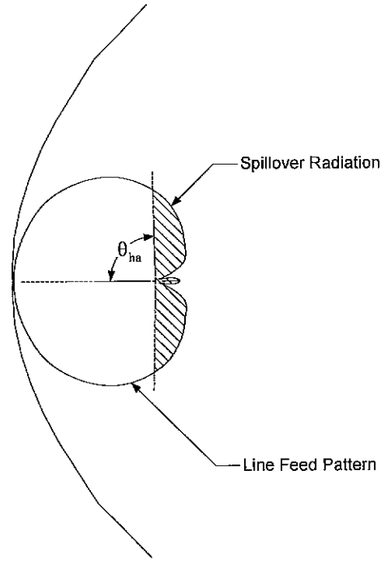

Figure 3.4 Line feed pattern illuminating the reflector in the transverse plane, showing the spillover radiation.

High spillover efficiency means most of the feed radiation is captured by the reflector. Spillover radiation from the ground corresponds to a temperature of around 300 K, whereas the sky temperature is around 3 K. Ground directed spillover increases the antenna temperature, described in Section 3.3.3, and thus degrades the system sensitivity.

Aperture blockage is caused by objects, usually metal, obstructing the reflector aperture and preventing radiation being collimated by the reflector. Objects include feed support struts and the feed ground plane. A Gaussian aperture illumination is assumed for the MOST beam model, as described in Section 2.5. However, realistic aperture blockage creates an illumination having amplitude nulls with a depth corresponding to the amount of blockage. When an aperture illumination with blockage is Fourier transformed, to obtain the reflector pattern, there is a decrease in gain and increase in beamwidth and sidelobe levels compared to an aperture illumination without blockage (Kraus 1966). In addition, for a centre-fed reflector, blockage causes a secondary scattering wave between the ground plane and reflector vertex, resulting in gain modulation with frequency and scan angle.

The MOST line feed is supported using single struts in the transverse plane, spaced at either 1 or 3 m intervals along the cylinder length. The feed support structure in the transverse plane is depicted in Figure 3.5, the width of each strut is around 0.14 m and the ground plane width is around 0.5 m. The dominant blockage effect is caused by the ground plane which shadows the support strut from incoming radiation and is the only aperture blockage considered.

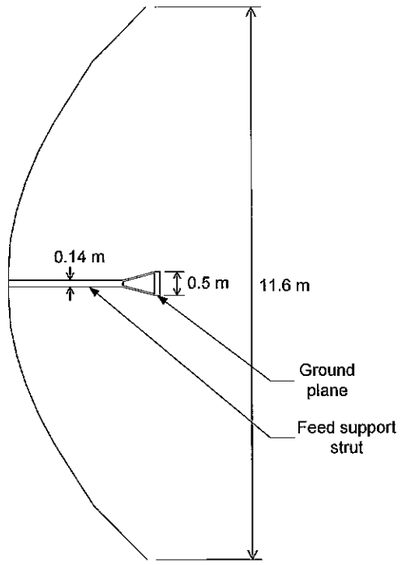

Figure 3.5 The MOST dimensions in the transverse plane showing the ground plane width dominates the blockage compared to the feed support strut.

The blockage efficiency can be calculated by:

$$\eta_{blk} = \left|1 - \Delta_b\right|^2 \tag{3.6}$$

The parameter Δ_b, represents the percentage of aperture being blocked by the ground plane width. An approximation can be made for Δ_b by assuming the co-polar pattern G_{cp} is relatively constant over the blockage region (Kildal 1984a):

$$\eta_{blk} = \left|1 - \frac{W_{gnd}}{D}\right|^2 \tag{3.7}$$

Where W_{gnd} is the transverse width of the ground plane.

Polarisation efficiency accounts for gain losses due to cross-polar radiation, which occurs in the plane orthogonal to the imaging (co-polar) polarisation and is calculated by:

$$\eta_{pol} = \frac{\int_{-\theta_{ha}}^{\theta_{ha}} \left|G_{cp}(\theta)\right|^2 d\theta}{\int_{-\theta_{ha}}^{\theta_{ha}} \left[\left|G_{cp}(\theta)\right|^2 + \left|G_{xp}(\theta)\right|^2\right] d\theta} \tag{3.8}$$

Although the polarisation efficiency indicates the polarisation performance of the feed, it does not provide sufficient pattern information to define the maximum cross-polar levels in the HPBW reflector pattern. These levels determine the polarisation imaging sensitivity, whereas the polarisation efficiency is used to describe the feed performance for design purposes. Another parameter known as the cross-polar ratio (XPR), described in Section 3.3.4, is used to describe the polarisation imaging sensitivity performance in the reflector pattern.

Longitudinal plane

Sub-efficiency parameters are different for the aperture in the longitudinal plane compared to the transverse plane. Radiation in this plane can modelled using a uniform line current assumption, described in Section 2.2. The feed taper efficiency in this plane, η_{Lt}, is determined by applying an amplitude weighting to the bay beams in the longitudinal direction. For example, if uniform illumination was required, equal amplitude would be applied to the bays beams and the taper efficiency, η_{Lt}, equals unity. The taper can be software controlled to optimise the weighting and hence the pattern, for a particular scientific observation and it is not analysed in this thesis.

Longitudinal plane spillover, η_{Lsp}, is negligible when the line feed is not electrically scanned, since the beams all point to the zenith. However, when the line feed is scanned, the bay beams closest to the reflector ends will detect spillover ground radiation at large scan angles, as shown in Figure 3.6. This effect can be reduced by placing an additional line feed, with elements terminated in matched loads, coupled with an additional reflector section at the ends of the instrument. Alternatively, the data corresponding to the baselines measured using the affected bay beams can be discarded. However, there is a trade-off in loss of sensitivity (u-v coverage). The affected baselines are the longest ones,

which provide the highest resolution, and the shortest baseline, which provide the best detection of extended emission. Both of these longitudinal spillover minimisation techniques are planned for SKAMP. Longitudinal plane blockage and polarisation efficiencies are the same as their equivalent transverse efficiencies since the cylindrical reflector is assumed infinite in the longitudinal direction.

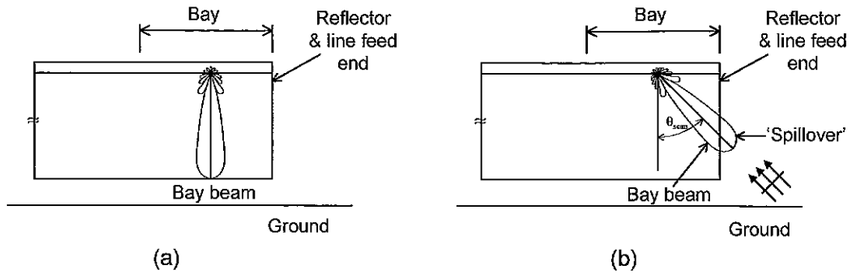

Figure 3.6 Side view of the MOST in the longitudinal plane, with the bay beam superimposed to show spillover for (a) 0° scan angle. (b) 45° scan angle.

Currently, the MOST has an effective area, A_{eff}, of approximately 9,000 m^2 (Mills 1981), with a physical collecting area of approximately 18,000 m^2, corresponding to an aperture efficiency of 0.5. This value will be used as the aperture efficiency design goal for the new SKAMP wideband line feed. Typical aperture efficiencies for reflector antennas range from 0.5 to 0.7 (Hansen 1966a).

The relationship between the effective area and system sensitivity, given in Equation 2.22, enables an investigation of how feed parameters affect the sensitivity through analysis of aperture efficiency. Sub-efficiencies, in Equation 3.2, can be individually analysed to determine the limiting parameter. A disadvantage of this analysis is that the feed sub-efficiency parameters are represented only as a percentage. Parameters that affect the imaging performance such as peak sidelobe and cross-polar levels must be determined from the radiation pattern, and are discussed in Section 3.3.3 and 3.3.4 respectively. Furthermore, sub-efficiencies will vary across the observation frequency and scan angle ranges. By modelling the variations subject to these operating conditions, appropriate corrections can be made using calibration techniques to recover image fidelity, as described in Section 3.4.2.

3.3.2 Bandwidth

The feed bandwidth is defined as the frequency range over which its impedance and radiation properties operate to an acceptable level set for the astronomy application. Frequency points used in defining the bandwidth are: the lower frequency (f_L), upper frequency (f_U) and centre frequency (f_c). These points are used to define the bandwidth as a percentage or a ratio, given by Equations 3.9 and 3.10. Either definition suffices, but it is usually expressed as a ratio (BW_r) for wideband applications and as a percentage (BW_p) for moderately wideband applications (Stutzman and Buxton 2000).

$$BW_p = \left(\frac{f_U - f_L}{f_c} \times 100 \right)\% \tag{3.9}$$

$$BW_r = \frac{f_U}{f_L} \tag{3.10}$$

A 300–1400 MHz frequency range is planned for SKAMP, which corresponds to a 4.7:1 ratio, with the maximum instantaneous bandwidth that can be processed being 100 MHz. Whilst the instantaneous bandwidth is limited by the sampling speed of the electronics, the feed bandwidth is limited by its impedance and radiation properties, which can be defined by its impedance bandwidth, scanning bandwidth and pattern bandwidth.

Impedance bandwidth is the range of frequencies over which the feed return loss is less than a pre-determined value. The return loss for an antenna is defined as the mismatch or ratio between the reflected and incident power, and represents the amount of signal detected at a particular frequency. For radio telescope feed designs, James (1992b) specifies an overall feed return loss of –15 dB (0.03 reflected power) as a desirable level. However, this specification is for a single feed system, whereas the line feed for the MOST consists of several thousand elements. The line feed return loss is affected by mutual coupling between elements and varies with scanning angle, resulting in a value greater than that specified by James (1992b). The specification used for the line feed design for SKAMP is –10 dB. Although signals can be received with a feed having a higher return loss, the signal strength is less, which degrades the signal-to-noise ratio (SNR) in the final image.

Scanning bandwidth can be defined as the range of frequencies over which there is no grating lobe in the field-of-view for a pre-defined maximum scanning angle. The grating lobe depends on element size, array spacing and scanning range, and was briefly described in Section 2.6. It differs from the grating rings caused by the periodic structure of the contiguous interferometer sections. A grating lobe for a line feed occurs in the field-of-view at θ_g, for a scan angle, θ_s, when the electrical element spacing, d/λ, satisfies the relation (Hansen 1998):

$$\frac{d}{\lambda} = \frac{n}{\sin\theta_s - \sin\theta_g} \tag{3.11}$$

Where n = the number of elements in the line feed.

The scanning bandwidth definition described by Stutzman and Buxton (2002) considers the element size, along the array direction (across the radiating aperture), at the lowest operating frequency and divides it by the element spacing at the maximum scan angle. A similar approach in Fisher (1996) presents the pattern bandwidth for a hexagonal array used in a reflector, in which the element size at the lowest frequency is divided by the spacing at which the grating lobe falls on the reflector edge. The method in Stutzman and Buxton (2002) is used in this thesis and is given by:

$$BW_{sc} = \frac{1}{l_{size}\left(1 + \sin\theta_{max}\right)} \tag{3.12}$$

Where θ_{max} = maximum scan angle

l_{size} = element size at lower frequency (wavelengths)

The effect of grating lobes on imaging is similar to that due to sidelobes and causes a reduction of SNR when a strong radio source drifts through the grating lobe peak. Depending on the area of sky being surveyed, sources may not appear in the grating lobe field-of-view during the observation interval. Grating lobes usually appear at large scanning angles for frequencies at the upper limit of the observation bandwidth, as the electrical element spacing increases. The imaging performance for MOST at large scan angles is already degraded by aperture foreshortening and gain reduction from scanning, so the grating lobe impact may be a secondary effect. Nevertheless from a line feed design perspective, the element size and type must be chosen to enable beam scanning and to maximise the scanning bandwidth in Equation 3.12. An investigation into the grating lobe across the scan angle range for the new SKAMP line feed is presented in Chapter 7.

Pattern bandwidth is the range of frequencies over which the co-polar feed illumination pattern, in the transverse plane, remains uniform in the angular collecting region subtended by the reflector. Uniform illumination implies no deep nulls, skewing or asymmetry in the pattern. Deep nulls in the illumination pattern cause phase errors in the reflector pattern which are manifested in the form of increased sidelobe levels and reduced aperture efficiency. Skewing and asymmetry in the illumination pattern produces an asymmetric reflector illumination that results in reflector pattern pointing errors. Specification of the pattern bandwidth comes from the line feed co-polar illumination pattern across the observation frequency and scan angle range. Slight non-uniform pattern variations due to unavoidable instrumental effects may be corrected through calibration.

All three line feed bandwidths depend on the type of element employed. A survey of the current state-of-the-art (SoA) phased array element technology is undertaken in Chapter 4, to assess whether the feed bandwidth can operate across the entire observing bandwidth and to identify limiting bandwidth parameters.

3.3.3 Antenna Temperature

A low system temperature is important because of the relationship between system temperature and sensitivity as given in Equation 2.22. Antenna temperature contributes through ground directed spillover, described in Section 3.3.1, and through radiation loss in sidelobes and back radiation seen in the reflector pattern. The back radiation refers to radiation directed in an angular region within ±30° of the direction opposite to the main beam, for either the feed illumination or reflector patterns. As described in Section 2.7, the calculation of antenna temperature requires knowledge of the feed illumination pattern, reflector pattern sidelobe levels and back radiation, not available for the current MOST beam model. This section describes the calculation of antenna temperature in the transverse plane, for a known feed illumination pattern (spillover temperature) and for a known reflector pattern (reflector temperature). Antenna temperature in the longitudinal plane results from spillover radiation and the bay beams can be weighted to minimise this contribution, as described in Section 3.3.1.

Spillover temperature can be estimated by considering the reflector pointing at zenith, as shown in Figure 3.7(a), with the hatched regions denoting ground directed spillover. The temperature contributions from the feed illumination pattern can be separated into the five regions listed in Table 3.2. The feed pattern outside the reflector edges, in the ground direction, receives ground noise at 300 K, corresponding to regions 1 and 2 in Figure 3.7(a), and sky noise at 3 K, corresponding to regions 3 and 4 in the same Figure. The spillover temperature is calculated by summing the temperature contributions from the five regions, shown in Figure 3.7(a) and dividing by the total gain:

$$T_{sp}(^{\circ}K) = T_{gnd}\frac{\int_{\theta_{hn}}^{90^{\circ}} G_{feed}(\theta)\,d\theta}{\int_{-180^{\circ}}^{180^{\circ}} G_{feed}(\theta)\,d\theta} + T_{gnd}\frac{\int_{-90^{\circ}}^{-\theta_{hn}} G_{feed}(\theta)\,d\theta}{\int_{-180^{\circ}}^{180^{\circ}} G_{feed}(\theta)\,d\theta} + T_{sky}\frac{\int_{-180^{\circ}}^{-90^{\circ}} G_{feed}(\theta)\,d\theta}{\int_{-180^{\circ}}^{180^{\circ}} G_{feed}(\theta)\,d\theta} + T_{sky}\frac{\int_{90^{\circ}}^{180^{\circ}} G_{feed}(\theta)\,d\theta}{\int_{-180^{\circ}}^{180^{\circ}} G_{feed}(\theta)\,d\theta} + T_{sky}\frac{\int_{-\theta_{hn}}^{\theta_{hn}} G_{feed}(\theta)\,d\theta}{\int_{-180^{\circ}}^{180^{\circ}} G_{feed}(\theta)\,d\theta} \tag{3.13}$$

Where G_{feed} = total feed gain (G_{cp} + G_{xp})

T_{gnd} = ground noise temperature (300 K)

T_{sky} = sky noise temperature (3 K)

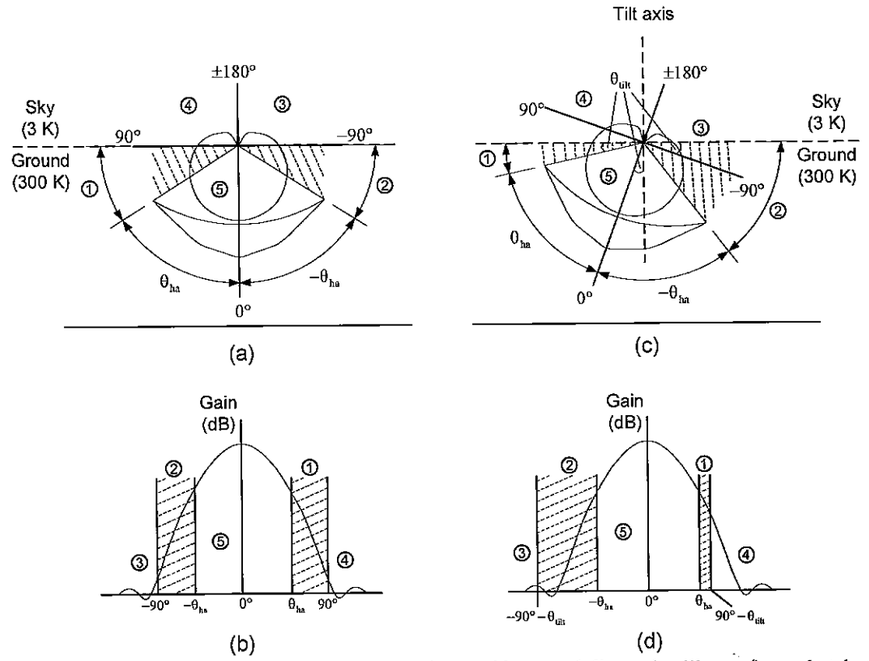

Figure 3.7 Temperature contributions from five regions, with ground directed spillover shown hatched. (a) Polar plot of pattern illuminating the reflector pointing at zenith (b) Cartesian plot of the feed illumination pattern for the reflector pointing at zenith. (c) Polar plot of pattern illuminating the reflector pointing at tilt angle, θ_{tilt}. (d) Cartesian plot of the feed illumination pattern for the reflector pointing at tilt angle, θ_{tilt}.

Region	Description	Integration Interval	Temperature (K)
1	Ground directed spillover	$[\theta_{ha}, 90°]$	300
2	Ground directed spillover	$[-90°, -\theta_{ha}]$	300
3	Sky directed spillover	$[-180°, -90°]$	3
4	Sky directed spillover	$[90°, 180°]$	3
5	Reflector directed radiation	$[-\theta_{ha}, \theta_{ha}]$	3

Table 3.2 Feed illumination pattern temperature contributions, for the reflector pointing at zenith, from the five regions shown in Figure 3.7(a).

The MOST uses mechanical tilting about its horizontal axis to steer the beam in the transverse plane. To calculate the spillover temperature for this operation, consider a mechanical tilt with the axis of rotation centred at the focal point, as shown in Figure 3.7(c). Again the feed temperature contributions are divided into five sections, listed in Table 3.3. The integration intervals for the temperature contributions are shifted by the amount of mechanical tilt angle, θ_{tilt}. The spillover contribution from region 1 disappears for the case when the tilt is large enough to pass through the horizontal axis centred at the focal point. Equation 3.14 describes the spillover temperature due to the application of mechanical tilt.

$$T_{sp}(°K) = T_{gnd}\frac{\int_{\theta_{ha}}^{90°-\theta_{tilt}} G_{feed}(\theta)\,d\theta}{\int_{-180°}^{180°} G_{feed}(\theta)\,d\theta} + T_{gnd}\frac{\int_{-90°-\theta_{tilt}}^{-\theta_{ha}} G_{feed}(\theta)\,d\theta}{\int_{-180°}^{180°} G_{feed}(\theta)\,d\theta}$$
$$+ T_{sky}\frac{\int_{-180°}^{-90°-\theta_{tilt}} G_{feed}(\theta)\,d\theta}{\int_{-180°}^{180°} G_{feed}(\theta)\,d\theta} + T_{sky}\frac{\int_{90°-\theta_{tilt}}^{180°} G_{feed}(\theta)\,d\theta}{\int_{-180°}^{180°} G_{feed}(\theta)\,d\theta} + T_{sky}\frac{\int_{-\theta_{ha}}^{\theta_{ha}} G_{feed}(\theta)\,d\theta}{\int_{-180°}^{180°} G_{feed}(\theta)\,d\theta} \quad (3.14)$$

Where G_{feed} = total feed gain (G_{cp} + G_{xp})

T_{gnd} = ground noise temperature (300 K)

T_{sky} = sky noise temperature (3 K)

Region	Description	Integration Interval	Temperature (K)
1	Ground directed spillover	$[\theta_{ha}, 90° - \theta_{tilt}]$	300 K: $90°-\theta_{tilt} > \theta_{ha}$ 0 K: $90°-\theta_{tilt} < \theta_{ha}$
2	Ground directed spillover	$[-90°-\theta_{tilt}, -\theta_{ha}]$	300 K
3	Sky directed spillover	$[-180°, -90° - \theta_{tilt}]$	3 K
4	Sky directed spillover	$[90° - \theta_{tilt}, 180°]$	3 K
5	Reflector directed radiation	$[-\theta_{ha}, \theta_{ha}]$	3 K

Table 3.3 Feed illumination pattern temperature contributions, for the reflector pointing at tilt angle θ_{tilt}, from the five regions shown in Figure 3.7(c).

Reflector pattern temperature is similar to the spillover temperature, but effects such as reflector curvature and aperture blockage are included in the calculation. It assumes the reflector pattern detects 300 K when pointing at the ground and 3 K when pointing at the sky. Figure 3.8(a) illustrates the reflector pattern temperature, which can be separated into three regions described in Table 3.4. Hatched regions in Figure 3.8 denote ground

directed spillover. When mechanical tilting is used to steer the beam, depicted in Figure 3.8(c), the ground directed angular region will shift by the tilt angle, θ_{tilt}, and the reflector pattern temperature becomes:

$$T_{ref}(°K) = T_{sky}\frac{\int_{-90°+\theta_{tilt}}^{90°-\theta_{tilt}} G_{ref}(\theta)\,d\theta}{\int_{-180°}^{180°} G_{ref}(\theta)\,d\theta} + T_{gnd}\frac{\int_{90°-\theta_{tilt}}^{180°} G_{ref}(\theta)\,d\theta}{\int_{-180°}^{180°} G_{ref}(\theta)\,d\theta} + T_{gnd}\frac{\int_{-180°}^{-90°+\theta_{tilt}} G_{ref}(\theta)\,d\theta}{\int_{-180°}^{180°} G_{ref}(\theta)\,d\theta} \quad (3.15)$$

Where G_{ref} = reflector gain

T_{gnd} = ground noise temperature (300 K)

T_{sky} = sky noise temperature (3 K)

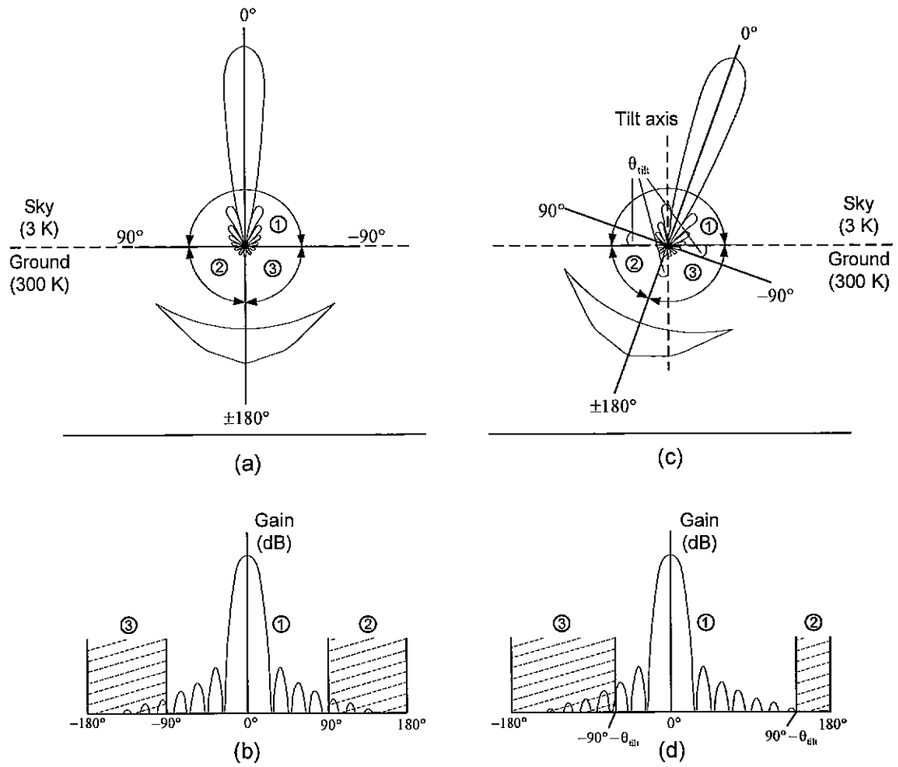

Figure 3.8 Reflector pattern temperature contributions, from ground and sky directed radiation. (a) Polar plot of the reflector pattern with the reflector pointing at zenith. (b) Cartesian plot of the reflector pattern for the reflector pointing at zenith. (c) Polar plot of the reflector pattern pointing at tilt angle, θ_{tilt}. (d) Cartesian plot of the reflector pattern for the reflector pointing at tilt angle, θ_{tilt}.

Region	Description	Integration Interval	Temperature (K)
1	Sky directed radiation	$[-90° + \theta_{tilt}, 90° - \theta_{tilt}]$	3 K
2	Ground directed radiation	$[90° - \theta_{tilt}, 180°]$	300 K
3	Ground directed radiation	$[-180°, -90° + \theta_{tilt}]$	300 K

Table 3.4 Temperature contributions, with the reflector pointing at tilt angle θ_{tilt}, from the five separate regions shown in Figure 3.8(c).

Although spillover and reflector temperature calculations account for the use of mechanical tilt, the radiation pattern in both cases will change as the line feed is electronically scanned in the longitudinal (East-West) plane. This is shown in Figure 2.7 for the measured reflector HPBW across the scanning range for the current MOST configuration. Because the antenna temperatures are determined from the radiation patterns, the feed illumination pattern, G_{feed}, and the reflector pattern, G_{ref}, in Equations 3.13–3.15 can be replaced with a pattern, $G(\theta,\theta_{scan})$, corresponding to a particular scanning angle, θ_{scan},. Integration limits in the transverse plane for the temperature calculations are unchanged because electronic scanning only changes the beam position in the longitudinal plane.

To determine how antenna temperature changes with scan angle for cylindrical reflectors, the performance of other cylindrical reflectors using scanning line feeds are investigated. When the line feed for a cylindrical reflector radar (Rahmat-Samii et al. 2005) is scanned to 30°, sidelobes for the simulated reflector patterns increase by 5 dB. For the EISCAT cylindrical reflector (Kildal 1984b), the aperture efficiency reduces for a scan angle of 25°. This is caused by an impedance mismatch from the grating lobe which increases the reflection loss, corresponding to an increased antenna temperature. A simulation of a scanned line feed for a symmetrically fed cylindrical reflector is described in Craeye (2005). Results are given for reflector patterns at 0° and 60° scan angles. The 60° scan angle reflector pattern shows an increase in back radiation in the order of 15 dB compared to 0° scan angle.

Spillover temperature calculated from the illumination pattern indicates the antenna temperature performance of a feed over a particular reflector angular region. Aperture blockage and reflector edge diffraction, which increase the sidelobe levels and back radiation, are not included in this calculation but affect the reflector pattern. Hence, spillover temperature can be used for the feed design whereas the reflector pattern temperature must be used to determine the antenna temperature of the interferometer beam. Another parameter that is used to evaluate the antenna temperature performance is the front-to-back ratio (F/B) in the feed illumination pattern. The F/B, shown in Figure 3.9, represents the ratio of the peak gain in the forward direction to the peak gain in the back radiation region (within ±30° of the direction opposite the main beam). For a particular element, the F/B provides an indication of the reflector antenna temperature. A feed pattern F/B of at least 25 dB will be used as a selection criterion for the SKAMP line feed element.

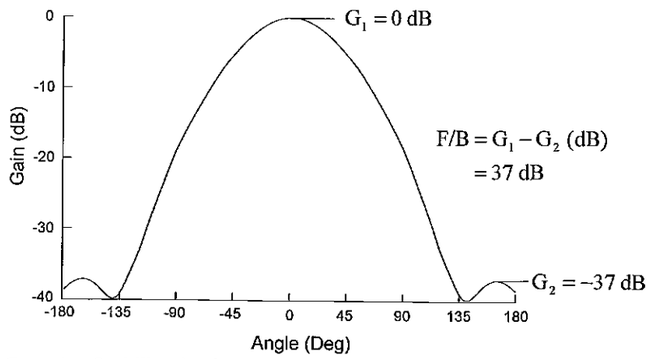

Figure 3.9 Cartesian feed illumination pattern, showing the calculation of the front-to-back ratio.

3.3.4 Polarisation

A single right-hand circular polarised feed (Mills and Little 1972) is used in the current MOST operation. Implementation of the new dual polarised line feed for the SKAMP upgrade will enable measurements that provide information on magnetic field structures and the astrophysics of radiation processes such as synchrotron and stimulated emission. This is important for understanding the physics of star formation and evolution, particle acceleration and the formation of galaxies, jets and black holes. Linear polarisation is produced in the synchrotron process by relativistic electrons moving in the interstellar magnetic field. Objects for which polarised emission is detected include supernova remnants, radio galaxies and pulsars. The theoretical maximum fractional polarisation of synchrotron radiation is 70% (Rohlfs and Wilson 1996). However, instrumental polarisation and Faraday rotation of the electric vector by the interstellar medium can reduce the detectable fractional polarisation. A goal of the SKAMP upgrade is to detect sources that are typically 5% polarised. For the present design study, the polarisation sensitivity is represented in logarithmic scale:

$$\sigma_p(dB) = 20\log_{10}(\sigma_p) \tag{3.16}$$

The SKAMP line feed must sense two orthogonal polarisations preferably with equal gain to measure all the Stokes parameters, necessary to characterise a polarised plane wave (Kraus 1966). An overall polarisation sensitivity of –26 dB is required to detect radio sources with fractional polarisations greater than 5%. Implementing a dual polarised line feed also improves the continuum sensitivity by a factor of $\sqrt{2}$.

Polarisation sensitivity can be determined by co-polar and cross-polar radiation patterns for a feed element with a particular polarisation alignment. A feed has a co-polar G_{cp} and cross-polar G_{xp} radiation pattern, shown in Figure 3.10(a). The co-polar radiation detects the desired signal, whereas the cross-polar radiation represents the signal received from the orthogonal polarisation. The parameter used to describe the polarisation sensitivity for the line feed is the cross-polar ratio (XPR), which is determined by dividing the co-polar by the cross-polar level occurring at the same angle, as shown in Figure 3.10(b). It is commonly expressed in decibels:

$$\mathrm{XPR}(\theta)\,[\mathrm{dB}] = |G_{cp}(\theta)| - |G_{xp}(\theta)| \tag{3.17}$$

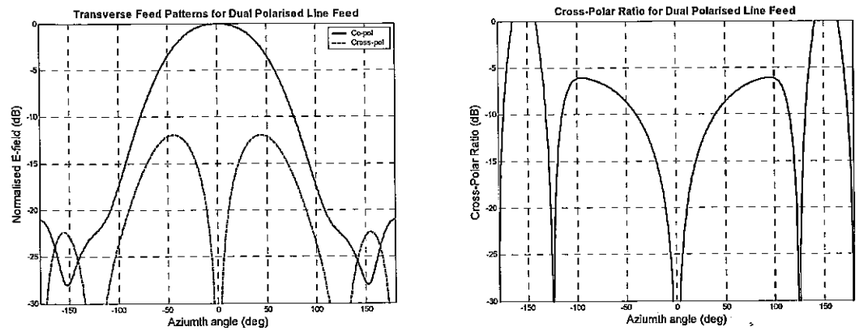

(a) (b)

Figure 3.10 (a) Typical transverse co-polar and cross-polar patterns for a dual polarised line feed. (b) Corresponding cross-polar ratio.

Although the line feed XPR can be determined separately, it is the XPR in the telescope imaging field-of-view that will define the overall polarisation sensitivity. For the MOST, the imaging field-of-view in the transverse plane is the angular region within the reflector pattern HPBW. James (1992a) specifies a peak XPR of –20 dB within the radio telescope field-of-view as a common requirement for polarisation imaging. However, SKAMP has a more stringent requirement of –26 dB for the detection of weak polarised radio sources at a level of 5%. Parameters that affect the polarisation sensitivity are the type of line feed element, polarisation orientation, the equality of gain between both polarisations and the electronic beam scanning.

The feed polarisation orientation describes the direction its electric field vector with respect to the array direction. Three common orientations are dual linear, dual circular and dual slant (±45°) polarisation. These orientations have different radiation and impedance performance across the scan angle range. Imaging linearly polarised synchrotron emission using a dual circular polarised feed requires software correlations to recover the Stokes parameters. With dual linear and dual slant feeds, signals are subtracted to recover the Stokes parameters. Large gain drifts between orthogonal polarisations will contribute to large errors, so system stability is important. The data from circular polarised feeds are less susceptible to gain drifts. However, the principal disadvantage for polarisation imaging using a line feed is maintaining polarisation purity while scanning over a wide frequency range.

Electric field vectors for dual linear polarisation are aligned longitudinal and transverse to the scanning plane. This alignment forces the cross-polar component to zero for 0° scan angle (Stutzman and Thiele 1998). In addition, the alignment enables the transverse illumination patterns to remain symmetric across the scan angle range. The orientation of the polarisations with respect to the middle of the ground plane, in the array direction, is not symmetric. This contributes to unequal transverse plane illumination patterns and unequal reflection coefficients for the orthogonal polarisations. Dual circular and dual slant polarisations are symmetric with respect to the middle of the ground plane and have equal illumination patterns and reflection coefficients for their respective polarisations. However, because dual circular and dual slant feeds are not aligned with the scanning plane they exhibit increased cross-polar radiation. This causes skewing of the feed illumination pattern for large scan angles, resulting in pointing errors in the reflector pattern. An investigation into the effect of beam skewing on the reflector pattern is presented in Section 8.3. Table 3.5 shows the characteristics of the three line feed polarisations on imaging performance.

Polarisation Orientation	Polarisation Performance	Pattern skewing when scanned	Equal Gain	System Stability Requirement
Dual Linear	Excellent	No	No	High
Dual Circular	Moderate	Yes	Yes	Low
Dual Slant	Moderate	Yes	Yes	High

Table 3.5 Comparison of three polarisation orientations against imaging requirements for the SKAMP line feed.

The selection of the SKAMP feed polarisation depends on the sensitivity that can be attained after calibration. However, there are RF performance parameters which are not easily corrected in the image analysis and remain dependent on the line feed design, such as the pattern skewing across the scan range. System stability can be improved by replacing the current IF and LO systems and gain equality can be improved via the

receiver electronics. The polarisation orientation that has optimum polarisation performance with no pattern skewing across the scan angle range is dual linear polarisation. Hence this polarisation orientation was chosen for the line feed design described in Chapter 6.

3.3.5 Engineering Considerations

The existing line feed for the MOST consists of over 7,000 elements, with a similar number required for the new SKAMP feed. A high volume feed design approach is required, with each element being low cost, low loss, robust with repeatable performance and easy to manufacture. This approach has already been used in converting the Molonglo Cross to the current MOST aperture synthesis telescope (Mills and Little 1972; Mills 1981). Another consideration for the line feed, is the operating environment, with temperatures at the telescope site varying between –15°C and +40°C throughout the year.

3.4 Line Feed Design Specifications

SKAMP line feed design requirements from Section 3.3 and their associated specifications are summarised in Table 3.6. The dependency is used to indicate whether the particular parameter can be obtained by analysing the feed separately from reflector or if it requires a combined analysis. Specifications denoted by a question mark (?) are unspecified as they depend on the type of radiating element chosen for the line feed. A parameter in Table 3.6 that is a consequence of wideband operation is the variation of phase centre across the instantaneous bandwidth. Certain wideband antenna elements radiate at different parts of their physical structure across the feed bandwidth corresponding to a varying phase centre. This is an undesirable characteristic for a reflector antenna feed because defocusing will occur if the phase centre for a given frequency is outside the focal region. A design scope is presented in the next section to describe limitations specific to the SKAMP feed design.

Antenna Parameter	Dependency	SKAMP Line Feed Specification
Aperture efficiency (A_{eff})	Reflector/Feed	0.5
Reflector pattern/Spillover temp (K)	Reflector/Feed	?
Polarisation sensitivity	Reflector/Feed	0.05 (–26 dB)
Feed beam pattern (HPBW)	Reflector/Feed	?
Impedance bandwidth	Feed	?
Return loss (dB)	Feed	–10 dB
Scanning bandwidth	Feed	?
Sidelobe/Grating lobe magnitude	Feed	–10 dB
Pattern bandwidth (MHz)	Feed	?
Angular scan range	Feed	$-60° < \theta_{scan} < -60°$
Dual polarisation	Feed	Yes
Phase centre variation	Feed	Small
Cost	Feed	Low
Construction complexity	Feed	Low
Repeatability	Feed	High
Element loss	Feed	Low

Table 3.6 Antenna requirements and corresponding specifications for the line feed design.

3.4.1 Design Scope

The SKAMP project will not upgrade the existing MOST mechanical structure, such as the reflector, feed support struts and mechanical tilt drive system. Of these components, the reflector and feed support struts affect the line feed design. The MOST reflector geometry has a deep taper with an $f/D = 0.26$, which places the focal point almost level with the reflector aperture. This has the advantage of reducing the amount of ground detected spillover. Figure 3.11 shows this angular spillover region compared with a reflector having an $f/D = 0.45$, representing a shallow taper. Although the MOST geometry reduces the spillover noise, it is difficult to illuminate the reflector with a high taper efficiency without compromising the antenna temperature. A feed pattern with a reasonable trade-off between spillover and taper efficiency is necessary to maintain acceptable aperture efficiency. The existing feed support struts will retain the ground plane width at 0.5 m, with a symmetric feed configuration maintained. This configuration contributes to aperture blockage causing increased sidelobe levels and a standing wave between the line feed ground plane and reflector vertex, which may ultimately limit the performance of any new line feed.

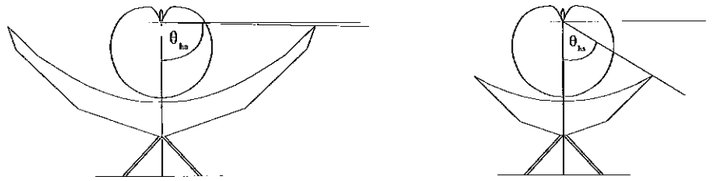

Figure 3.11 Spillover radiation from feed illumination for (a) MOST, $f/D = 0.26$, $\theta_{ha} = 88°$. (b) Reflector geometry, $f/D = 0.45$, $\theta_{ha} = 58.1°$.

For current synthesis observations with the MOST at large scan angles, the gain reduces due to aperture foreshortening and tapering in the element pattern. The measured gain variation in the scanning plane (EWGF) for the MOST, shown in Figure 2.6, at the scan limits (±60°) reduces the received signal to 0.25. Any improvements in the line feed performance may be limited at large scan angles with minor impact on the overall imaging sensitivity. The level of line feed performance degradation on the imaging sensitivity is still to be evaluated. Because polarisation and wideband imaging for cylindrical reflector aperture synthesis radio telescopes has not been attempted, calibration strategies are not yet proven. However, the line feed parameters that may be calibrated are described next.

3.4.2 Calibration

Calibration of the existing line feed parameters was described in Section 2.6, with the main requirements being whether a given parameter has a characterisable variation that is repeatable over the synthesis interval. This Section describes the calibration requirements and the level of correction achievable for the SKAMP 3 line feed.

Calibration requires accurate modelling of the radiation pattern across the scan angle range. SKAMP has a 100 MHz instantaneous bandwidth, and hence the level of variation of the line feed parameters across this bandwidth determines the amount of calibration required. For polarisation imaging, the co- and cross-polar radiation patterns across the scanning and operational bandwidth are required. Post-observing processing may improve the polarisation sensitivity in the final image, but high levels of cross-polar radiation in the reflector pattern contribute to inaccuracies in measured data. From a feed design viewpoint, it is important to identify the level of calibration that can be attained for a particular performance parameter. For example, if the gain variation with scan angle can be corrected through the data analysis rather than through modifications in the design, then it is better to optimise other line feed parameters that cannot be so easily corrected. This is the case for the polarisation imaging accuracy which is limited by the XPR in the reflector beam and can only be improved in the line feed design. Line feed antenna temperature effects such as spillover, sidelobes and element losses also affect performance and must be optimised in the design as shown in Table 3.7.

Line Feed Parameter	Calibration	Design Optimisation Requirement
Aperture efficiency (A_{eff})	No	High
Reflector pattern/Spillover temp	No	High
Reflector pattern polarisation sensitivity	No	High
Polarisation imaging	Yes	Medium
Impedance bandwidth	No	High
Sidelobe level	No	High
Pattern bandwidth	No	Medium
Gain variation with scan angle	Yes	Medium
Element loss	No	High
Phase centre variation	No	High

Table 3.7 List of line feed parameters describing whether they can be calibrated or require design optimisation.

3.5 Summary

An overview of the SKAMP upgrade to the MOST was described, which provides a background to the line feed developed in this thesis. SKAMP will extend the current MOST scientific capability by enabling spectral line, radio polarimetric and improved continuum sensitivity imaging. Key technologies which enable the SKAMP line feed development come from advancements in phased array elements for military, satellite and wireless communications which have dual polarisation and wideband performance requirements. To evaluate the suitability of this technology, a set of line feed engineering parameters and their impact on the imaging performance were established. Dual linear polarisation orientation was selected for its superior polarisation performance and pattern symmetry at large scan angles compared to dual circular and dual slant configurations. However, the selected configuration has unequal transverse illumination patterns for the orthogonal polarisations. Generic line feed specifications and their dependent parameters were presented in Table 3.6. Specifications for parameters such as impedance bandwidth, pattern bandwidth, scanning bandwidth and polarisation sensitivity were not presented because they are dependent on the type of element selected for the line feed design. An investigation into the state-of-the-art phased array element technology to determine a suitable element for the SKAMP line feed is presented in the next Chapter.

Chapter 4

Wideband Feed Options for SKAMP

Growth in military and wireless communications sectors has increased the development of new phased array technology, in particular for wideband dual polarised antenna elements. This technology can be utilised to extend the scientific capability of existing radio telescopes. The SKAMP upgrade to the Molonglo Observatory Synthesis Telescope (MOST) was described in Sections 3.1 and 3.2. A key new technology is the development of a wideband dual polarised phased array line feed. Performance specifications for radio telescopes differ from non-astronomy applications. For example, radio telescopes are receive-only and transmit requirements such as high power handling capability and low passive intermodulation are unnecessary. Line feed engineering requirements specific to the SKAMP project were discussed in Section 3.3 and are shown in Table 3.6.

Section 4.1 presents a description of antenna performance terminology followed by a survey of the current state-of-the-art antenna technology. The selection of a suitable phased array element technology for SKAMP is discussed in Section 4.2. Limitations of the selected feed element are addressed and a solution to overcome them is described in Section 4.3.

4.1 Antenna Technology Survey

Design parameters to describe the characteristic performance of particular antenna types are the orientation of the electric field vector to the plane of measurement, back radiation, front-to-back ratio, method of feeding the antenna, scan impedance and scan element pattern.

Radiation patterns are usually characterised in *planes* with respect to the orientation of the electric or magnetic field vector of the measured antenna. Patterns can be measured in the **E**-plane (along the electric field), **H**-plane (along the magnetic field) and the plane ±45° to the electric field. *Back radiation* refers to the radiation within ±30° of the direction 180° from the main beam pointing. *Front-to-back ratio* or F/B is the ratio of the maximum main beam electric field intensity divided by the maximum electric field intensity in the back radiation region, as described in Section 3.3.3.

Antenna elements must have the appropriate aperture dimensions and feeding network to ensure they can radiate and receive an electric field at the specified frequency. A discrete element requires an aperture which has an excitation current that is equal in amplitude, with a phase difference of 180° across the aperture. A device that can provide this excitation is a *balun*, which is a balanced-to-unbalanced transformer. This device takes

an unbalanced transmission medium, such as a coaxial line or microstrip, and transforms it to a balanced medium, producing two outputs that are equal in amplitude with a 180° phase difference between them. A coaxial balun from Stutzman and Thiele (1998) is shown in Figure 4.1. The quarter wavelength of line, at the centre frequency, from point b to c has the effect of cancelling the current on the outside of the coaxial line, such that the currents I_1 and I_2 are equal with a 180° phase difference across point a and b. Another type of device used to facilitate radiation for a discrete element is known as a coupler. To feed an element, such as a dipole, a hybrid coupler is used which has a single coaxial input and two coaxial outputs having equal amplitudes with a phase difference of 180° between them. Directly connecting the outputs to a pair of dipole arms creates the necessary balanced feeding condition for radiation to occur.

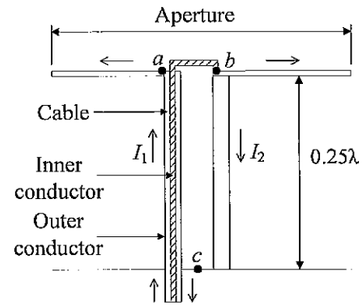

Figure 4.1 Coaxial balun connected to a dipole element. (Stuztman and Thiele 1998).

To obtain an indication of performance for an array design, a single element can be analysed in isolation before implementation in an array. However, when the elements are arranged in an array, the performance will change due to mutual coupling from surrounding elements and a new set of array analysis parameters are required. These parameters are the *scan element pattern* and *scan impedance*, which are explained in more detail in Section 6.1.1.

The scan element pattern represents the array gain variation with scan angle and is determined by exciting a single element in an array with the other elements terminated in the characteristic impedance. Polarisation performance with scan angle for a particular array, at a specific frequency, can be determined by analysing its co- and cross-polar element patterns. The scan element impedance represents the impedance of an array as a function of scan angle. It is measured by exciting all the elements with the correct amplitude and phase to produce a main beam pointing at a particular scan angle. Resonances that occur in the scan impedance at particular scan angles represent a loss of power at that scan angle. These resonances are element construction and array geometry effects and are manifest in the form of blind angles caused by surface waves and grating lobes. Blind angles are scan angles at which no power is received and correspond to nulls in the scan element pattern, which mean a loss in radiation efficiency and sensitivity at the particular scan angle. Both array performance parameters are analysed for the operational scanning planes of the array.

4.1.1 Log Periodic

A log periodic antenna has dimensions that scale logarithmically to achieve equivalent operation over a large frequency range. One type of log periodic antenna is a sheet trapezoidal toothed-antenna (DuHamel and Ore 1959), which consists of two arms with teeth tapered away from the feeding point, as shown in Figure 4.2. The periodic teeth variation causes the antenna to radiate at different points along the arm at different operating frequencies, which produces frequency independent radiation across a wide frequency range.

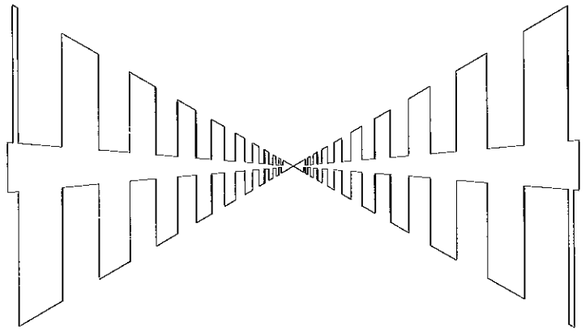

Figure 4.2 Planar view of a singly polarised log periodic trapezoidal toothed antenna

Log periodic antennas are used in single-feed reflector antennas for applications requiring large operating bandwidths, such as the dual linear polarised feed for the Allen Telescope Array (ATA); which operates over the frequency range 0.5–11.0 GHz (Engargiola 2002). Dual polarisation was achieved by placing an arm on each triangular-face of a square based pyramid and feeding each pair of opposing arms using a wideband balun. This feed had high polarisation and taper efficiencies, with the spillover limiting the overall aperture efficiency (Ericsson et al. 2003). Increased back radiation caused the low spillover efficiency with F/B ratios being around 15 dB. The feed pattern XPR was around –25 dB indicating good polarisation sensitivity (Engargiola 2002). System temperature was reduced by connecting a low noise amplifier (LNA) directly after the balun to minimise path loss, and cryogenically cooling the receiver to minimise receiver noise.

Although the log periodic antenna has wideband radiation performance, the periodicity results in a phase centre variation across the operating frequency range. For the ATA, this variation is minimised by using a mechanical actuator to re-focus the feed. An alternate wideband feed design for the ATA presented in Olsson et al. (2004) avoids the use of a mechanical actuator by implementing a design that reduces phase centre variation. Instead of using log periodic teeth, log periodic dipole arms are used and arranged in an inverted pyramid configuration to maintain a constant electrical dipole arm height above the ground plane across the frequency range. This configuration, shown in Figure 4.3 for a single polarisation, resulted in a relatively constant phase centre and reduced back radiation.

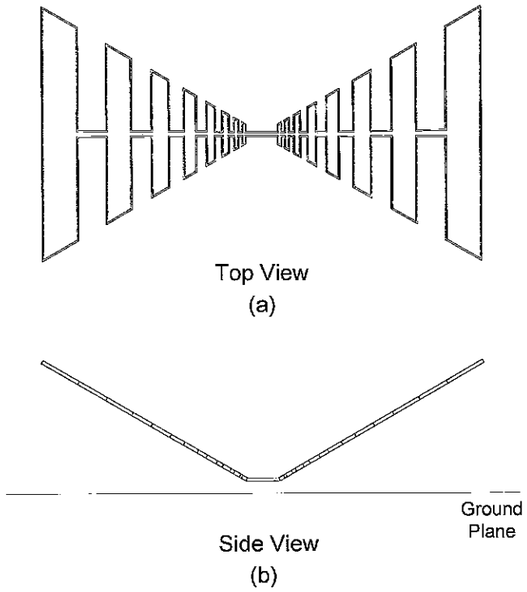

Figure 4.3 Single-polarisation inverted log periodic antenna. (a) Top view. (b) Side view.

4.1.2 Wideband Dipole

A dipole consists of two collinear electrical conductors or arms separated by a gap. A voltage source is placed across the gap, to create a current distribution on the arms which is equal in magnitude with a 180° phase difference between each arm. A combined arm and feed gap length of 0.5λ is selected for resonance, to enable maximum radiation in the plane orthogonal to the length. A ground plane can be placed behind the arms for unidirectional radiation. Because of the resonant arm length, the impedance bandwidth is low: typically 8–16% (Stutzman and Thiele 1998). Dipoles used as feed elements for existing cylindrical reflector radio telescopes are listed in Table 1.2, with impedance bandwidths around 4%.

A method used to broaden the impedance bandwidth of the resonant dipole is to increase its arm area. The bandwidth increases because the currents flowing on the arms are distributed over a larger area, corresponding to a reduced impedance variation. A design with increased arm dimensions to improve the impedance bandwidth is referred to as a wideband dipole in this thesis. One such design is the bow-tie element shown in Figures 4.4(a) and 4.4(b), where the two arms extend from the feed point to form a triangle. The bow-tie element described in Bailey (1984) was designed to operate over a 510–660 MHz frequency range. The element comprised two triangular arms etched on printed circuit board (PCB) and fed using a coaxial balun. The combined arm length was 0.3λ, placed 0.375λ above a ground plane at the centre frequency. An impedance bandwidth of 1.5:1 was attained, with the measured radiation patterns at 500 MHz and 650 MHz exhibiting uniform co-polar radiation in the forward direction in the principal radiation planes. Cross-polar radiation levels were low, with a XPR < –27 dB at boresight. Back radiation levels were high at the upper frequency limit, with F/B levels around 20 dB.

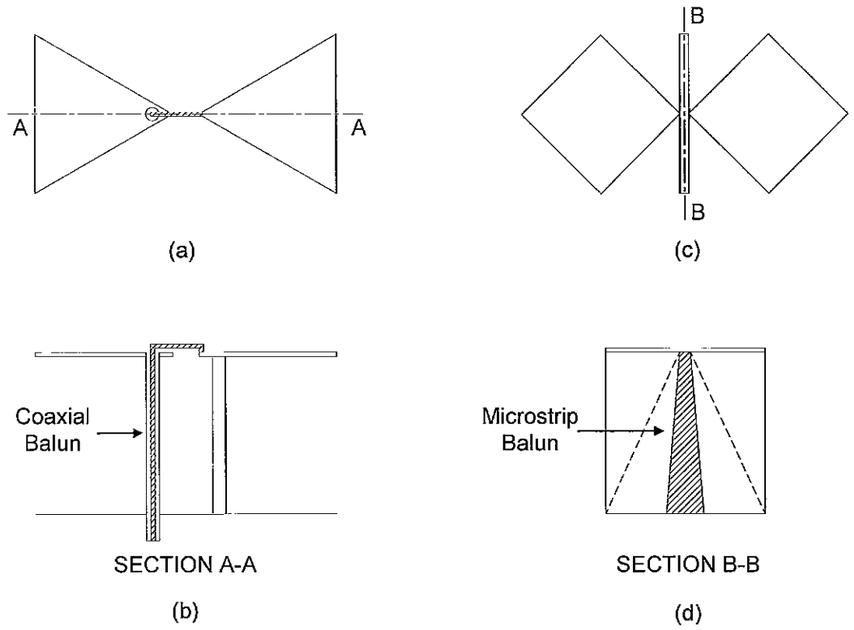

Figure 4.4 Bow-tie element with a coaxial balun feed: (a) top view and (b) side view. Wideband dipole with a microstrip balun feed: (c) top view and (d) side view.

To further increase the impedance bandwidth of a wideband dipole, a microstrip balun can be used as shown in Figures 4.4(c) and 4.4(d). This balun has a larger impedance bandwidth than the coaxial balun because the cable impedance is fixed whereas the microstrip balun can be adjusted to match its impedance to an arbitrary reference impedance, such as to the LNA. This result is described in Akhoondzadeh-Asl et al. (2005). A tapered microstrip balun was used to achieve an impedance bandwidth of 2.5:1 over a 4.9–12.2 GHz frequency range. The combined arm length was 0.8λ, placed 0.09λ above an electromagnetic band gap ground plane at 5 GHz. The element length is roughly twice that of a bow-tie antenna because the arms are in a diagonal arrangement. The co-polar radiation patterns were uniform in the forward direction over a frequency range of 3.7–6.8 GHz, corresponding to a 1.8:1 pattern bandwidth. Patterns at frequencies > 6.8 GHz show deep nulls and increased back radiation. A XPR of –25 dB is obtained at boresight across the pattern bandwidth.

Kim et al. (2003) describes a wideband dipole fed by a tapered microstrip balun with a 2.6:1 impedance bandwidth over a 1.6–4.2 GHz frequency range. The combined dipole arm length was 0.5λ, placed 0.38λ above the ground plane at the centre frequency. Co-polar radiation patterns show nulls in the forward direction at the upper frequency range, approximately 25°–30° from boresight, which limits the pattern bandwidth to 1.9:1 over a frequency range of 1.6–3 GHz. Microwave absorber is placed above the ground plane to reduce the nulls at these frequencies. However, this contributes to the antenna loss. A disadvantage of the microstrip balun implementation is a slight pattern asymmetry resulting from the fringing fields on the microstrip board. This effect is seen for co-polar

patterns at the upper operating frequency range for both aforementioned microstrip balun fed wideband dipole designs.

The previous paragraphs describe singly polarised wideband dipoles. However, a dual polarised dipole is required for SKAMP. This can be achieved by arranging two singly polarised dipoles orthogonal to each other, as depicted in Figure 4.5. This configuration is known as a crossed dipole and can be oriented on a linear ground plane to produce dual linear or dual slant polarisation.

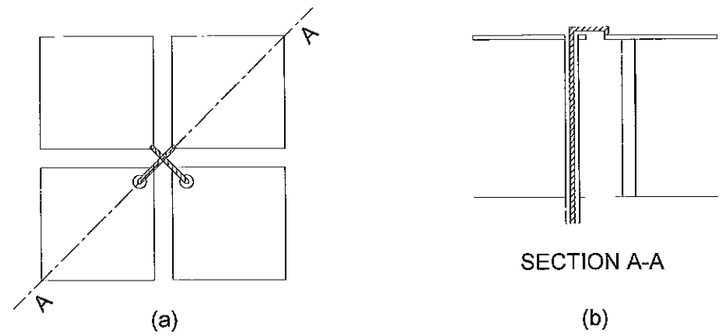

Figure 4.5 Dual polarised wideband dipole. (a) Top view. (b) Side view.

A wideband dual polarised dipole described in Perruisseau-Carrier et al. (2003) has an impedance bandwidth of 3.5:1 and a pattern bandwidth of 3:1. A large impedance bandwidth is obtained by using fractal-like cuts for the dipole arms, which are printed metallisation on both sides of a dielectric substrate. Instead of a balun to feed the dipole arms, a hybrid coupler is connected directly to the arms to provide the correct feeding. The hybrid coupler used had a single unbalanced coaxial input and two coaxial outputs with equal voltages and a 180° phase difference between them. The outputs are connected to a pair of arms to create the correct feeding for a single dipole polarisation. Hence, two hybrid couplers are required for dual polarisation operation. The dipole arm height above the ground plane was 0.25λ and its diagonal arm length was 0.4λ at the lowest operating frequency. A layer of microwave absorber placed at the ground plane base improved the pattern bandwidth. At the upper frequency limit, the co-polar patterns show large nulls whereas the lower frequency patterns show large levels of back radiation, with an average F/B of 12.5 dB. The polarisation purity was good, with XPR < –25 dB at boresight across the band, although somewhat less for the lower operating frequencies.

Another type of wideband dual polarised dipole element, the fourpoint element described in Suh et al. (2003), has a 2:1 impedance bandwidth over 1.5–3 GHz and a 1.8:1 pattern bandwidth. The impedance bandwidth of this design is improved with an indentation between the arms to reduce the impedance variation at the upper frequency limit. A hybrid coupler provides the correct excitation. The dipole arms are printed on a single-sided PCB, with the arm length being 0.35λ at the lower frequency and positioned 0.25λ above the ground plane at the centre frequency. Co-polar patterns in **E**- and **H**-planes have a HPBW of 60° and 80° respectively at the centre frequency. Measured radiation patterns at the centre frequency show uniform radiation in the forward direction, good polarisation purity, with XPR < –30 dB, and low back radiation levels, with F/B > 30 dB.

Shaped metallised plates can be placed between the dipole element and ground plane, as shown in Figure 4.6, to increase the impedance bandwidth. Wong and King (1972) describe the use of shaped sleeves placed above and below a crossed dipole element, with a triple stacked circular sleeve configuration providing the largest impedance bandwidth. This configuration had a 2:1 impedance bandwidth, and a pattern bandwidth of 1.8:1 over 450–800 MHz. Back radiation levels were increased at the low frequency end, with a F/B of 20 dB, compared to the upper frequency range, with F/B of 30 dB. Cross-polar levels were low, with XPR levels < –25 dB at boresight. Suh et al. (2005) present a PCB wideband dual polarised dipole design with a tuning plate printed on the opposite side of the board layer with the four printed dipole arms. The tuning plate was printed on the element as described in the previous paragraph (Suh et al. 2003). A star shaped tuning plate produced an impedance bandwidth of 2.3:1, which improves the bandwidth by 26% compared to the design without a plate. The effect of the plate increased the impedance bandwidth at the upper frequency limit. The pattern bandwidth was 2:1, with the HPBW being around 60° and 90° in **E**- and **H**-planes across the band. Back radiation levels at the low to mid frequency range, had F/B > 24 dB. However the back radiation increased at the high frequency limit, with F/B around 18 dB. Cross-polar levels were low, with XPR levels < –30 dB across the pattern bandwidth.

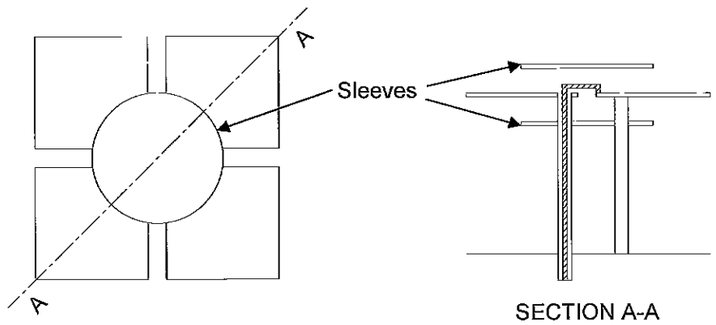

Figure 4.6 Dual polarised wideband dipole with metallic sleeves for bandwidth enhancement. (a) Top view. (b) Side view.

From the survey of the different wideband dual polarised dipoles, the pattern bandwidth is the limiting parameter, not the impedance bandwidth. The impedance bandwidth increases if shaped metallic plates are placed optimally above or below the dipole arms, as in Wong and King (1972) and Suh et al. (2005). The pattern bandwidth is limited by deep nulls in the co-polar patterns for singly and dual polarised wideband dipoles at their upper operating frequency. Increased levels of back radiation were exhibited at the lower and upper limits of the pattern bandwidth depending on the design. However, the cross-polar radiation levels produced by this design are low, which meets the SKAMP polarisation sensitivity specification. The element size is typically less than 0.5λ at the centre frequency which allows illumination of the reflector along its entire length and facilitates electronic beam scanning.

The hybrid coupler feeding method used for the dual polarised wideband dipoles described in Suh et al. (2003) and Perruisseau-Carrier et al. (2003) increases the antenna noise temperature and cost compared to a balun feed. For the dipole described in

Perruisseau-Carrier et al. (2003), the coupler has an average noise figure of 0.7 dB (http://catalog.tycoelectronics.com/), corresponding to a noise temperature of 51 K. A low loss, low cost element favours a cable balun (Bailey 1984) or a microstrip balun (Akhoondzadeh-Asl et al. 2005). However, hybrid coupler feeding is easier to implement than balun feeding. In addition, couplers connect to the arms individually whereas a balun is connected across a pair of arms and a cross-over is required to provide dual polarisation. Feeding the dipole arms correctly is complex, particularly when low cross-polar radiation is required.

Dipole elements have been commonly used as feeds for cylindrical reflector radio telescopes as listed in Table 1.2. They were the element of choice for frequencies below 1 GHz because of their ease of construction, uniform radiation patterns, low back radiation and good impedance characteristics. However, these feeds only operated with a single polarisation and had a narrow operating bandwidth of several percent.

4.1.3 Wideband Patch

A microstrip patch antenna consists of a metallised patch etched on a dielectric substrate with metallised backing or ground plane, shown in Figure 4.7. For a rectangular patch, the dimension L in Equation 4.1 is chosen to be resonant at the design frequency. The patch can be fed in several ways using probe, microstrip, aperture and proximity coupled feeding. Because the patch is resonant, its impedance bandwidth is limited to several percent (Garg et al. 2001).

$$L = \frac{c}{2 f_r \sqrt{\varepsilon_{re}}} \tag{4.1}$$

Where $c = 2.99 \times 10^8 \, ms^{-1}$

f_r = resonant frequency

ε_{re} = relative dielectric constant of the substrate

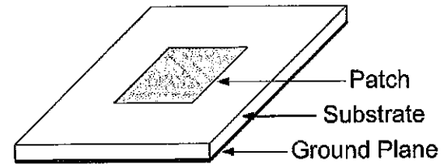

Figure 4.7 Microstrip patch antenna configuration.

Wideband microstrip antennas use aperture coupled feeding and stacked patches (Targonski et al. 1998) to increase the impedance bandwidth of a single patch to more than 2:1. This type of antenna, illustrated in Figure 4.8, uses a microstrip line to feed an aperture or slot which excites a resonant patch and an additional patch is placed or stacked on top of the resonant patch. The effect of using an aperture to feed the resonant patch creates a double-tuned impedance response because the aperture itself is chosen to be resonant. Another patch 'stacked' above the resonant patch provides an additional resonance, which further increases the impedance bandwidth. The dimensions of the slot, resonant patch, stacked patch and height of the patches are adjusted so their respective

resonances create a large impedance bandwidth. One such an antenna is described in Ghorbani and Waterhouse (2002).

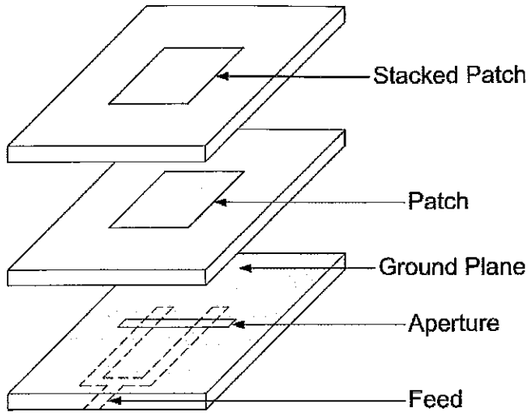

Figure 4.8 Aperture coupled stacked patch antenna configuration.

Dual polarised operation is achieved by using the existing configuration shown in Figure 4.8 with a second slot rotated 90° with respect to the first slot. Both are fed with microstrip lines positioned orthogonally. Implementation of a symmetric feed network for both polarisations, on the same board, requires an air bridge for one of the feed lines to prevent contact and incorrect excitation. A symmetric feeding network provides similar radiation patterns and input impedance on both polarisations, and minimises cross-polar radiation levels. Sanford and Tengs (1996) describe a dual polarised aperture coupled patch, shown in Figure 4.9. This design uses symmetric feed lines on two separate board layers, thus eliminating the air bridge requirement. Relevant phase delays for the two orthogonal microstrip feed networks were implemented to produce either dual linear or dual circular polarisation. A single square patch with 0.3λ width at the centre frequency was used. The impedance bandwidth for this design was 1.5:1 for both polarisations. The co-polar **E**- and **H**-plane patterns had uniform radiation across the impedance bandwidth, with a 60° HPBW in both planes. Back radiation levels were high, due to the resonant aperture used for feeding, with F/B ratios being around 16 dB.

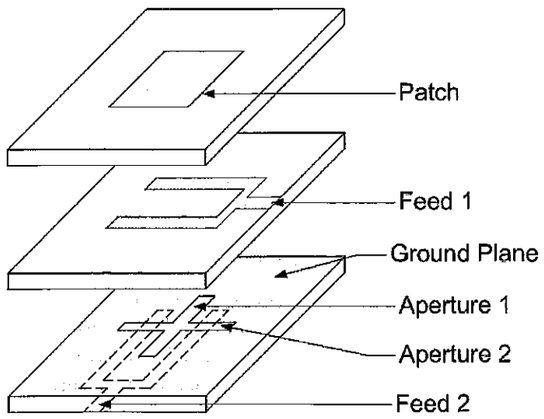

Figure 4.9 Dual polarised aperture coupled patch antenna with symmetric microstrip feed networks for both polarisations.

Ghorbani and Waterhouse (2004) increased the impedance bandwidth and reduced the back radiation of the dual polarised aperture coupled patch described in Sanford and Tengs (1996), by using a stacked patch configuration with a reflector. An impedance bandwidth of 1.7:1 and a pattern bandwidth of 1.7:1 were attained. A square patch with 0.3λ width at the centre frequency was used. Back radiation levels were minimised by using a metallised cross-shaped reflector, with 0.6λ length at the centre frequency, printed on a dielectric substrate placed behind the aperture. The F/B levels were around 20 dB and XPR levels were < –22 dB at boresight. Waterhouse et al. (2002) also use an additional substrate layer placed behind the aperture to reduce the back radiation. Metallised square-shaped reflectors positioned behind the resonant aperture are printed on the additional layer, which reduced the back radiation levels by 15 dB across the operating frequency range. Instead of using a reflector printed on substrate placed to reduce the back radiation, Nystrom and Karlsson (1997) use a closed metallic box placed behind the feed aperture. Back radiation levels reduced, with F/B levels being around 25 dB across the operating frequency range. Another approach to reduce the back radiation levels of an aperture coupled patch antenna is to place the antenna above a ground plane and shape its profile. Such designs are described in Lindmark et al. (1999) and Wong and Luk (2003), which use shaped ground planes and flanges to minimise the currents that contribute to the back radiation. Lindmark et al. (1999) use a genetic algorithm to modify the ground plane shape for optimum F/B, to reduce back radiation levels by 10 dB. Wong and Luk (2003) place two flanges either side of the radiating element with vertical slots cut out periodically along the flange to reduce back radiation levels by around 3 to 10 dB.

Aperture coupled patch antennas have the advantage of repeatable design through printed circuit board manufacturing techniques. This allows the integration of the first stage LNA and electronics, which minimises losses by avoiding the use of interconnecting cables. The patch size is < 0.5λ at the centre frequency which enables the element to be used as a scanning line feed. A disadvantage of this element is the moderate level of construction complexity to achieve large impedance bandwidths. The dual polarised aperture coupled stacked patch design in Ghorbani and Waterhouse (2004) requires five low loss substrate layers and three foam layers to achieve an impedance bandwidth of 1.7:1. Whilst this design may be acceptable for certain applications and frequency ranges it would be impractical for SKAMP. Lindmark (1997) presents a one layer dual polarised aperture coupled antenna, which simplifies the construction. Air bridges are avoided by using asymmetric microstrip feed lines for the slot. However, this produces different radiation patterns and input impedances on each polarisation and also limits the impedance bandwidth to 1.1:1 on one polarisation.

Although a balun is not required to feed the patch, the use of a resonant aperture coupled feed increases the back radiation. Techniques have been developed to minimise the back radiation from the aperture, but it is difficult to suppress this radiation across the whole bandwidth. Choosing a back radiation minimisation technique is dependent on the operating frequency. Placing a box behind the aperture is impractical at higher frequencies because of the small box dimensions. At low frequencies, an additional substrate layer containing a reflector patch becomes large and expensive. Ground plane modification techniques are effective for back radiation reduction but can be frequency dependent, therefore limiting wideband performance.

A microstrip line feed design for a cylindrical reflector radar is described in Huang et al. (2005). Singly polarised line feeds were designed for two operating bands, 13 GHz and 35 GHz. The operating bandwidth was 10 MHz, which corresponds to a bandwidth of less than 1% at both frequencies of operation. Microstrip antennas were chosen as the feed element for their ease of construction, low weight and size compared to other types of antennas at the same operating frequency. The element spacing used was 0.6λ at the centre frequency, with a scan angle range of ±35°. Radiation patterns for the line feed showed XPR levels around –22 dB in the main beam and the first sidelobe peak was –20 dB for both operating frequencies. This feed is deemed unsuitable because it is single polarisation and has narrow bandwidth.

4.1.4 Densely Spaced Arrays

Densely spaced arrays (DSA) have element spacing at approximately their physical width. The design of these arrays uses mutual coupling effects caused by the close spacing to extend input impedance and scanning bandwidths. Close spacing is achieved using an element with a narrow width across its aperture. For example, an element with a metallised geometry that tapers out from the feed point to the aperture, as shown in Figure 4.10. Common elements used in DSA are the tapered slot antenna (TSA) and the rabbit ear antenna (REA).

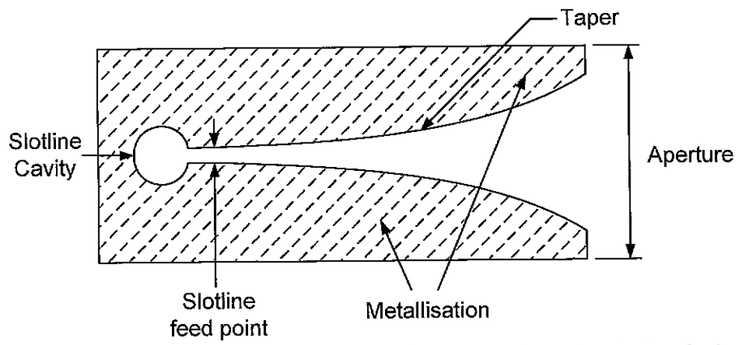

Figure 4.10 Tapered slot antenna, showing the tapered geometry from the slotline feed point to the aperture.

A TSA element, shown in Figure 4.11(a), is constructed using PCB with a microstrip slotline at its base which is tapered outward to form an aperture. A balun feeds the slotline near the base of the element to provide the correct excitation. The taper shape from the slotline feed to the aperture can be stepped, linear or exponential and is selected such that the input impedance matches the free space impedance at the aperture. This provides wideband impedance and radiation performance.

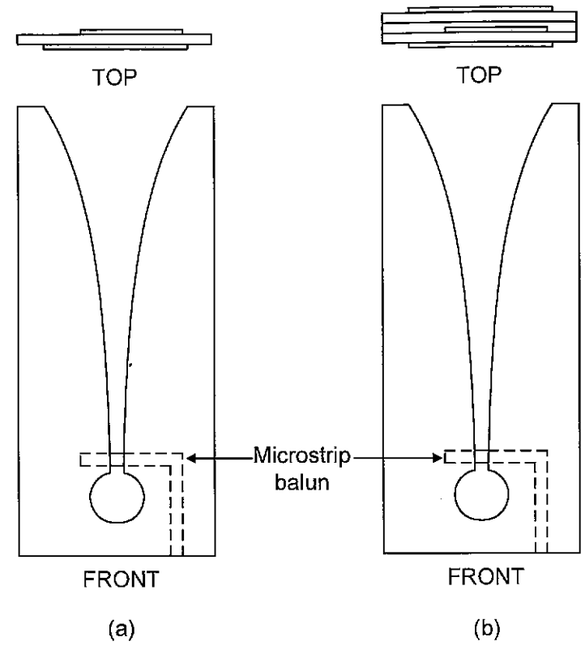

Figure 4.11 (a) Single layer printed circuit board TSA with a microstrip feed balun. (b) Double layer printed circuit board TSA with a stripline feed balun.

The construction allows accurate taper design and facilitates an interface with the first stage electronics. However, this design has high levels of cross-polar radiation, with an average XPR of –5 dB across the operating bandwidth for the TSA (Langley et al. 1993), caused by the open microstrip feed line balun radiating and contributing to cross-polar radiation. An alternative feeding network uses a stripline feed, whereby the balun is placed between two conducting layers to reduce the line radiation. As a result, two printed circuit boards are required as shown in Figure 4.11(b) and described in Langley et al. (1996). This element has an impedance bandwidth of around 4:1 and has 0.3λ aperture width and 0.8λ element length at the lowest operating frequency. Co-polar **E**- and **H**-plane HPBWs varied from 40°–60° across a 2.3:1 frequency range. Polarisation performance was improved compared to a microstrip fed TSA, with XPR levels varying from –32 to –15 dB across a 3:1 frequency range, with the levels < –20 dB for a 2.6:1 range. Co-polar **E**-plane radiation patterns exhibited nulling and squinting, whereas the **H**-plane patterns were uniform. Back radiation levels were high, with average F/B around 10 dB.

Dual polarised TSA operation is achieved by interleaving pairs of orthogonal elements form a lattice when placed in an array. This technique is known as 'egg-crating' (Hansen 1998) and is shown in Figure 4.12 for TSA elements interleaved at the edges of each element.

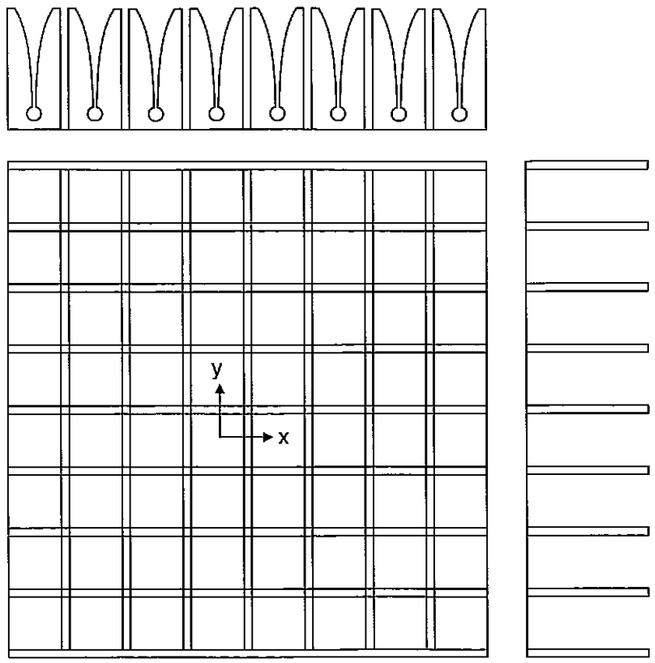

Figure 4.12 Dual polarised 8 × 9 TSA array, with a frontal view and side view of the x-directed polarisation.

Chio and Schaubert (1999) describe the performance and construction of an 8 × 9 dual polarised TSA array. The array used PCB techniques, with the elements interleaved at the element edges. The scan impedance bandwidth was 4:1 across a scan angle range of 0°–50°. The upper scan angle limitation of 50° is due to resonances that occur in the scan impedance. These resonances were removed by modifications to electrically connect the two stripline ground plane layers. This increased the scan impedance bandwidth to 5:1 across the same scan angle range. The element had 0.1λ aperture width and 0.36λ length at the lowest operating frequency. **E**- and **H**-plane co-polar scan element patterns showed a slight nulling in the forward radiation direction, with the null depth being larger at lower frequencies. This suggests the patterns are being influenced by finite edge effects, which are more prominent at lower frequencies. Cross-polar radiation is low at 0° scan angle in both **E**- and **H**-planes, with XPR levels < –26 dB across the band. These levels degrade at larger scan angles with the worst case being in the **H**-plane, showing –12 dB at 60° scan angle. Element patterns in the plane ±45° to the electric field showed nulling across the frequency range. XPR levels were < –20 dB at 0° scan angle, with the levels becoming 0 dB at 60° scan angle, implying the polarisations cannot be resolved at this scan angle.

A disadvantage of the TSA element used in the dual polarised array geometry, in Figure 4.12, is that its balun feeding arrangement does not permit an $n \times n$ array. This is because feeding requires the orthogonal elements to be interleaved at their edges, to avoid the baluns touching, resulting in an $n \times (n+1)$ array. In addition, this balun arrangement prevents coincident phase centre location for both polarisations. A design, shown in Figure 4.13(a), that addresses these limitations is described in Pickles et al. (2007). It uses two slotline cavities fed using a pair of microstrip baluns with a common feed point

to excite a single polarisation. Both baluns are oriented to produce the necessary surface currents on the element for radiation to occur. A dual polarised 6 × 6 array is shown in Figure 4.13(b), which has orthogonal elements interleaved at their centre represented by the dotted line in Figure 4.13(a). The feeding allows a symmetric array configuration, with coincident phase centre location, which results in an improved polarisation performance compared to the single balun fed array element, shown in Figure 4.12.

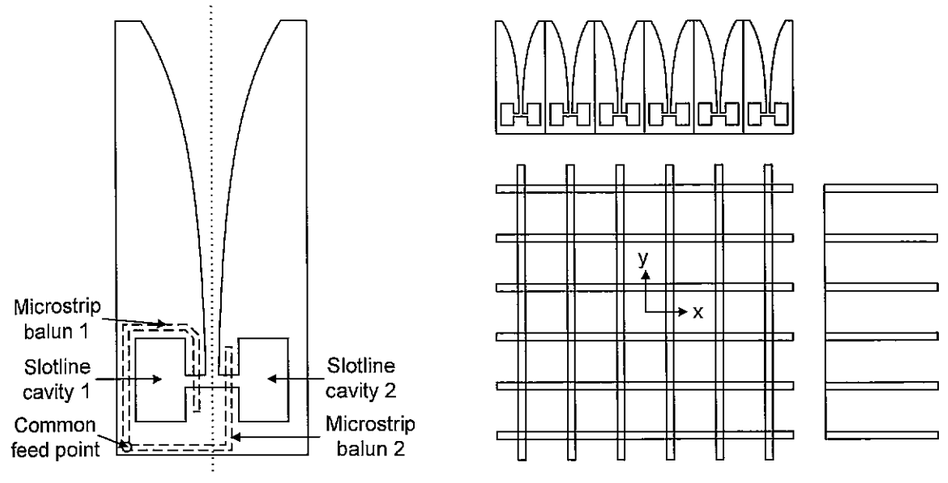

Figure 4.13 (a) Coincident phase centre TSA element. (b) 6 × 6 Dual polarised coincident phase centre TSA array, with a frontal view and side view of the x-directed polarisation.

Another type of element used in DSA is known as the rabbit ear antenna (REA), which is shown in Figure 4.14. This element has a tapered slotline, which is flared outwards to produce a pair of dipole arms at the aperture (Lee and Livingston 1993). The tapered slotline enables wideband impedance and radiation bandwidths. In this design, the slotline is fed by a coaxial connector, with the baluning action provided by electrically connecting the inner conductor to one arm and the outer conductor to the other arm. This element has an impedance bandwidth of 36:1, with 0.3λ aperture width and 0.5λ element length at the lowest operating frequency. Because the element length is less than the TSA, the magnitude of the longitudinal surface currents is reduced which corresponds to lower cross-polar radiation.

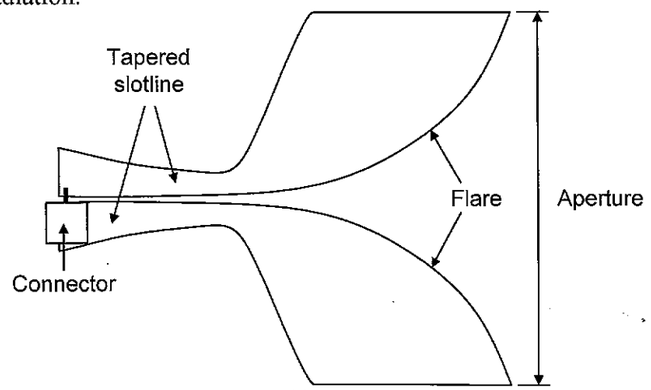

Figure 4.14 Rabbit ear element (REA).

When the REA is arranged in an array, the bandwidth reduces due to mutual coupling. A dual polarised 9 × 9 REA array described by Lee et al. (2003) was measured for element patterns over a 4.3:1 bandwidth. Co-polar **E**- and **H**-plane patterns showed minor nulling in the forward direction. XPR levels at 0° scan angle were < –23 dB in **E**- and **H**-planes across the bandwidth. At 60° scan angle, the XPR levels were < –20 dB in the **E**-plane and < –12 dB in the **H**-plane. In the plane ±45° to the electric field, co-polar patterns again showed minor nulling in the forward direction. XPR levels were < –25 dB at 0° scan angle and < –4 dB at 60° scan angle. Nulling in array element patterns is prominent for small arrays due to edge effects and is reduced by increasing the array size or by using dummy elements. A 25 × 25 REA array shows a reduction in element pattern nulling in the forward direction, across the measured frequency range (Lee et al. 2004). Resistive film was placed on the edges of the dipole arms and connected to the ground plane, to reduce the effect of resonances from inter-element coupling.

Using PCB construction for TSA and REA arrays enables accurate element design and ease of manufacture. However, the excitation of unwanted surface waves occurs at particular scan angles. These waves indicate power is dissipated in a direction other than the main beam, causing a resonance in the scan impedance bandwidth. Other disadvantages of using PCB for densely spaced arrays are: soldering vulnerability, dielectric losses and the high cost of low loss substrate material. A TSA array design that uses solid metallic (aluminium) construction rather than PCB construction has been described in Holter (2007). Solid, bullet-like aluminium elements replace the metallisation in the printed circuit board TSA design. This design eliminates the need to electrically connect the two ground plane layers and eliminates the possibility of impedance resonances resulting from incorrect electrical grounding.

Implementation of a densely spaced array for a reflector antenna feed represents the state-of-the-art in array technology for radio telescopes. Limitations of densely spaced arrays compared to a single-pixel feed are: increased feed design complexity, increased noise and mutual coupling, increased electronics and increased computing requirements for signal processing. Using densely spaced arrays enables the possibility of multiple fields-of-view or beams, with a constant gain. Calibration techniques can account for reflector surface distortion and strut blockage. The beam can also be optimised to provide low sidelobes, high gain and increased polarisation purity. Advancement in antenna, electronics and computer technologies over the last decade have made the implementation of a densely spaced array feed feasible.

Research efforts are presently aimed at evaluating the use of densely spaced arrays for future telescopes. For example, the 8 × 9 dual polarised TSA focal plane array on the Westerbork synthesis telescope uses a conjugate power analysis approach (Ivashina et al. 2004). A 20-element dual polarised TSA prototype telescope feed has been constructed and measured for element patterns in Veidt (2007). An 8 × 8 linearly polarised TSA feed for a parabolic reflector as an interferometer is presented in O'Sullivan (2006) and development of associated electronics for a DSA are described in Bunton (2007). Issues requiring investigation include the accurate modelling of the array performance, reduction of the element construction complexity and cost, development of electronics and signal processing software to manage the enormous data rates.

4.1.5 Sinuous Antenna

A sinuous antenna consists of four zigzag-shaped arms tapered outwards from the feed centre, as shown in Figure 4.15. An appropriate feeding network connected to the arms provides either dual circular or dual linear polarisation. The arms are printed as metallisation on PCB material, with a cavity mounted behind the element to provide directional radiation. The arms are tapered in a zigzag shape, similar to a log periodic antenna, to provide wideband impedance and pattern bandwidth. However, in contrast to a log periodic antenna, the radiating arms of the sinuous antenna are positioned on a planar surface.

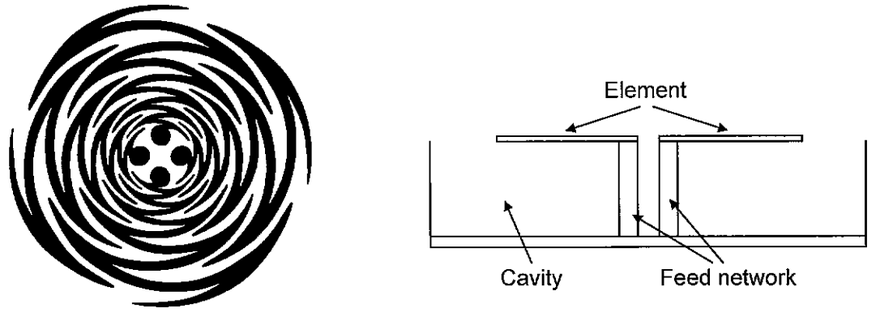

Figure 4.15 Sinuous antenna. (a) Top view. (b) Side view, showing the feeding network and cavity.

A sinuous slot antenna element design presented in Begaud et al. (2000) had an impedance bandwidth of 10:1 for one polarisation and 12:1 for the orthogonal polarisation subject to a –6 dB return loss criteria. Singh et al. (2005) describes the measured radiation performance of a sinuous antenna over a 9:1 bandwidth. **E**- and **H**-plane co-polar patterns showed uniform radiation in the forward direction and low back radiation levels across the bandwidth. A cavity placed behind the element reduced the back radiation, improving the F/B to over 25 dB. Pattern squint appeared in both measurement planes for frequencies at the upper limit of the measured bandwidth. Polarisation performance improved with increasing frequency, with XPR levels varying from –30 to –10 dB across the band. Bowen and Mayes (1994) investigated the half-power beamwidth variation of a dual circularly polarised sinuous antenna over a 2:1 bandwidth. The variation in beamwidth for left-hand circular polarisation (LHCP) in both **E**- and **H**-planes was 70°–80° and for right-hand circular polarisation (RHCP), it was 52°–100°. Element size of a sinuous antenna is around 0.5λ at the lower operating frequency (Tripp and Wang 1991).

Advantages of the sinuous antenna are its ease of manufacture using PCB, and large impedance and pattern bandwidths. Its implementation on a planar surface reduces the phase centre variation across the operating bandwidth. Dual circular polarisation can be produced for a sinuous antenna. However, only a single polarisation can operate at a given time and switching is required between LHCP and RHCP. For simultaneous measurement using both polarisations, dual linear or dual slant polarisation must be used for the front-end and dual circular polarisation can be obtained later in the signal processing by using an appropriate scaling network. The feeding technique to excite the sinuous antenna is similar to the wideband dipole feeding described in Section 4.1.2.

When the sinuous antenna is placed in an array, its size restricts the useable scanning range, before grating lobes appear in the field-of-view.

Sinuous antennas have been used in a feed array for a parabolic dish telescope. Fisher and Bradley (2000) describe the use of a 19-element sinuous antenna array feed for a parabolic dish, which was designed to operate over a 1.4:1 bandwidth with 0.5λ element spacing at the lowest operating frequency. The element spacing was chosen such that the array elements fully sampled the focal fields of the parabolic dish, meaning the array pattern produces no grating lobe responses in the field-of-view. The array element spacing used for a parabolic dish is determined by its subtended half-angle and acceptable grating lobe level at this angle (Fisher 1996) and is not subject to the line feed scanning requirement given in Equation 3.12. Electrical beam scanning is not usually a requirement for a feed array in a parabolic dish because the mechanical positioner provides beam steering.

4.1.6 Fractal Antenna

A fractal antenna consists of an element geometry with self-similar shapes. The antenna design is created using a standard geometry followed by application of fractal iterations to modify the geometry. Figure 4.16 shows a comparison between a square loop and an equivalent fractal element. Fractal iterations produce multiple resonances which make the antenna behave similarly to a frequency dependent antenna (Cohen 1997). Designing antennas with fractal geometry has the advantage of producing the performance of a standard antenna, using a smaller geometric size. In array designs, this enables closer element spacing which increases scanning bandwidth and reduces mutual coupling effects. An element size reduction of 0.36 was obtained for a fractal loop compared to an equivalent square, allowing a seven element fractal antenna linear array with 0.35λ spacing to occupy the same physical length as a five element square loop with 0.5λ spacing (Gianvittorio and Rahmat-Samii 2000).

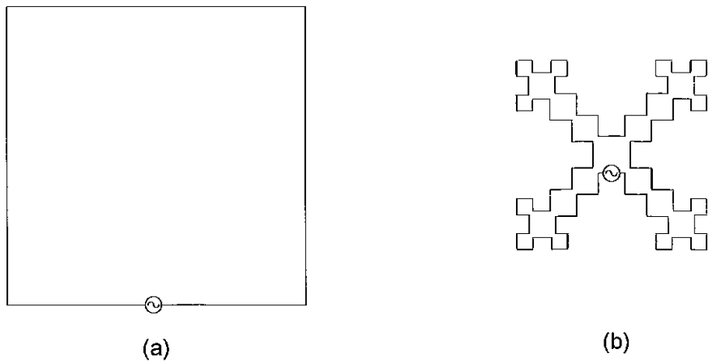

Figure 4.16 (a) Square loop antenna. (b) Equivalent fractal loop antenna to (a).

Fractal geometry can be applied to the radiating element geometry of standard dipole and patch designs to extend the pattern bandwidth. Thus, the method of feeding and achieving dual polarisation for fractal elements is similar to the standard dipole or patch design. A dual polarised fractal dipole element using the singly polarised geometry

presented in Gelman et al. (2004) is shown in Figure 4.17, which can be fed with a network similar to the one shown in Figure 4.5. Puente-Baliarda et al. (1998) compare the **E**- and **H**-plane radiation patterns of a fractal dipole antenna against an equivalent bow-tie antenna over an 8.9:1 bandwidth. The fractal dipoles have similar radiation patterns over the band, whereas the bow-tie patterns vary. However, the impedance bandwidth has several nulls across the band, with their positions determined by the fractal geometry. Fractal geometry was used for the dipole arms in the element described by Hee et al. (2003). The impedance bandwidth was 2:1, limited by deep nulls across band. **E**-plane radiation patterns were presented over a 5:1 bandwidth. Pattern nulling occurs in the forward direction in the mid to high frequency band. Back radiation levels increase at the band centre, showing an F/B of 10 dB. XPR ranges from –20 to –12.5 dB across the band.

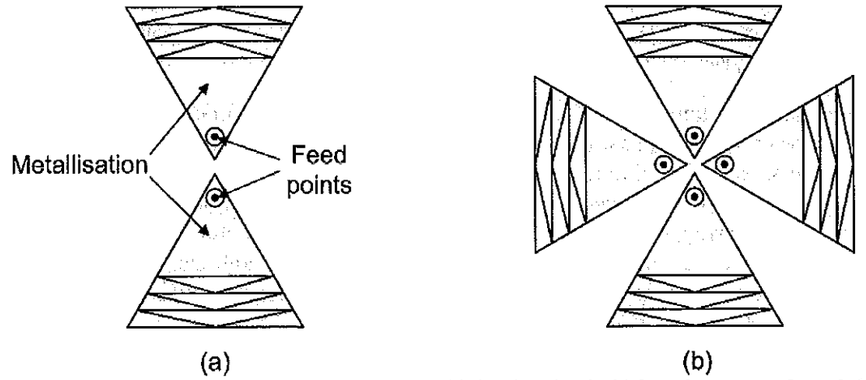

Figure 4.17 (a) Singly polarised dipole element, with third-order Sierpinski fractal geometry from Gelman et al. (2004). (b) Dual-polarised fractal dipole element based on (a).

Microstrip patch fractal antennas have been implemented by Anguera et al. (2004) and Nahshon et al. (2005). Both of these designs start with a triangular microstrip patch, then fractal geometry is applied to create a modified first-order Sierpinski fractal antenna in Anguera et al. (2004) as shown in Figure 4.18(a), and to create a second-order 'snowflake' fractal antenna in Nahshon et al. (2005) as shown in Figure 4.18(b). In the design of Nashon et al. (2005), the element is used in a singly polarised 9 × 9 array. Standard microstrip impedance bandwidth enhancing techniques were used to extend the bandwidth. These techniques include introducing an air gap between the ground plane and the patch and using a sleeve-type feeding pin to reduce the pin inductance. The array was placed in a metallic cavity to improve the polarisation performance. Scan impedance bandwidth for the central element was 1.6:1, for a return loss specification of –8 dB. Element patterns for the **E**- and **H**-planes showed a relatively flat gain response out to scan angles of ±45°, with a gain variation of 2 dB across this range. Polarisation performance in the **E**-plane showed XPR levels < –25 dB for scan angles within ±45° and levels < –13 dB in the **H**-plane across the same scan angle range.

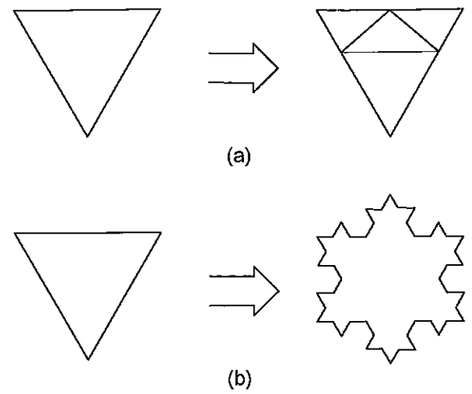

Figure 4.18 (a) Microstrip patch element converted to a first-order modified Sierpinski fractal geometry, from Anguera et al. (2004). (b) Microstrip patch element converted to a second-order 'snowflake' geometry, from Nashon et al. (2005).

Because fractal antennas use a design technique applied to a particular antenna type, such as patch or dipole antennas, they are not considered as a separate type of feed element. The advantages of fractal antennas include improved radiation performance over a wider frequency range and a reduced element size to increase the scanning bandwidth and field-of-view in an array configuration. However, the use of fractal geometry introduces resonances at frequencies corresponding to the number of iterations. So if a continuous impedance bandwidth is required, the geometry needs modification to ensure that it satisfies the return loss specification.

4.2 Element Selection

There are several parameters in Table 3.6, which are determined by the type of element used in the line feed. These parameters are the impedance bandwidth, scanning bandwidth and pattern bandwidth. The aim of this Section is to compare these parameters for current antenna element technology, reviewed in Section 4.1, and select one for the SKAMP line feed prototype. Table 4.1 shows a comparison of possible antenna elements, with requirements similar to those from Stutzman and Buxton (2000), in their comparison of wideband elements for phased arrays. It is assumed that all the elements described can be arranged to sense dual linear polarisation. Engineering factors for the SKAMP line feed include low cost, low construction complexity, robustness, high repeatability and simple manufacturing techniques. The element size refers to the antenna dimension across its radiating aperture in the array direction. The scanning bandwidth represents the range of frequencies over the SKAMP angular scan region for which a grating lobe does not appear in the field-of-view, as calculated by Equation 3.12.

The antennas in Table 4.1 are compared for operation in a single element environment rather than in array, following most of the configurations described in the literature. Array performance data such as the scan element pattern and scan impedance were not available for all elements. The array design methodology is to firstly evaluate a single element and then assess its performance in an array environment. Although the mutual coupling changes the antenna performance in an array, the single element is a good indicator of 'best case' conditions. Fractal antennas are not listed in Table 4.1. All the

feed parameters listed are scalable to different frequency ranges, except for the 'engineering complexity' which only refers to the SKAMP 300–1400 MHz frequency range.

Antenna type	Impedance bandwidth (Return Loss < –10 dB)	Element size (λ_H)	Scanning bandwidth (±60°)	Pattern bandwidth	HPBW variation (°)	XPR (dB) at boresight	Engineering complexity
Log periodic	22:1	>1.0λ	-	-	~45°	< –25 dB	High
Wideband dipole	2:1	0.35λ	1.5:1	1.8:1	60°–90°	< –30 dB	Low
Wideband patch	1.7:1	0.4λ	1.3:1	1.7:1	60°–70°	< –22 dB	Moderate
Densely Spaced Array (TSA)	5:1 (Scan Impedance)	0.1λ	5.3:1	-	-	< –26 dB (Scan element pattern)	High
Sinuous	2:1	0.5λ	1.1:1	9:1	45°–80°	< –10 dB	Low

Table 4.1 Comparison of different line feed elements against line feed requirements.

The log periodic antenna is included, because it represents the state-of-the-art in wideband single-pixel feed technology. However, it is unsuitable for SKAMP since its element length across the aperture is greater than 1λ. When arranged in an array and electrically scanned, grating lobes appear in the field-of-view, which will limit the imaging capability. Because the antenna is constructed using a pyramid structure, its phase centre varies across the operating frequency, which is undesirable.

Wideband dipole elements have impedance and scanning bandwidths less than the SKAMP operating frequency range. The feed bandwidth is limited by the scanning bandwidth. Impedance tuning techniques, such as the addition of sleeves depicted in Figure 4.6, can be used to increase the impedance bandwidth but the scanning bandwidth is fixed by the element size. Using a fixed-size ground plane for unidirectional radiation affects the pattern bandwidth at the lower operating frequency limits. The height of the element above the ground plane becomes electrically small and therefore, the currents on the element and ground plane do not contribute in phase, which reduces the radiation efficiency. At the higher frequency limits, the element arms become electrically large and nulls form in the forward direction of the radiation pattern. Advantages of this element include excellent polarisation performance and low back radiation across the pattern bandwidth. Dipole elements are easy to manufacture, have a simple economical construction, especially for the SKAMP frequency range. They have already been used in singly polarised line feeds for several cylindrical reflector antennas, as described in Chapter 1. Feeding dual polarised dipoles using hybrid couplers will increase the antenna losses, so a low loss, wideband dual polarised balun must be developed.

Wideband patch elements, such as an aperture coupled stacked patch, have an impedance bandwidth and scanning bandwidth less than the SKAMP operational frequency range. The horizontal dimension of the element size (Ghorbani and Waterhouse 2004) is taken as the length of the cross-shaped reflector ($0.4\lambda_L$) which is placed behind the coupling aperture, rather than the patch size, ($0.2\lambda_L$). This is because the cross-shaped reflector will be the limiting dimension when the element is placed in an array. The scanning bandwidth is better without the cross-shaped reflector, but the back radiation increases by

10–15 dB. For the SKAMP operation it is preferable to use the cross-shaped reflector because increased back radiation increases the antenna temperature. Although design techniques described in Section 4.1.3 can be used to minimise the back radiation, the levels remain relatively high compared to other element types due to the aperture coupled feeding technique. A pin-feeding technique was presented for a microstrip fractal element in Section 4.1.6. However, it was only used to feed a single polarisation, whereas a dual polarised feeding network offers a greater design challenge due to the increased number of feeding pins and limited space on the ground plane board for the connectors. An advantage of this element is its good polarisation performance. The use of PCB construction enables integration of first stage electronics, conformal and accurate design, and repeatability in performance. The engineering complexity is moderate because five substrate layers and three foam layers are required to achieve a wide impedance bandwidth. Because low loss dielectric substrates are required for SKAMP, this increases the element cost. As a result, microstrip patch antennas are commonly used in arrays only at higher frequencies, where the wavelengths are smaller and manufacturing costs reduced.

Densely spaced arrays, using tapered slot antenna elements have an impedance bandwidth and scanning bandwidth that will operate over the SKAMP frequency range. The pattern bandwidth and half-power beamwidth are not shown in Table 4.1 because these parameters are dependent on the array configuration and how the outputs from the elements are combined for beamforming. DSA advantages include wideband impedance and scanning properties. Polarisation performance is excellent at boresight, but degrades when the array is scanned. Although using PCB manufacturing offers design accuracy, resonances may occur from insufficient electrical connectivity between metallisation layers. As a result, the solid metallic construction described in Section 4.1.4 is preferable. The engineering costs for a DSA for the SKAMP line feed are high due to the greater number of elements required. The current MOST line feed uses elements spaced 0.6λ at the centre frequency, whereas TSA elements would be spaced 0.3λ at the centre frequency. In addition, an increase in the signal processing requirement also increases the design complexity for the RF beamformers, correlator and other systems in the signal pathway. SKAMP requires a line feed, whereas a DSA uses planar or 2D array geometry. TSA elements can be implemented in a line feed, but only a finite number of elements can be arrayed in the transverse direction before aperture blockage becomes a problem, particularly for the centre-fed reflector configuration of the MOST. The wideband impedance bandwidth properties may then be affected due to the small number of elements arrayed in the transverse direction. Craeye (2005) simulates the radiation performance of a linear TSA array in a cylindrical reflector with three elements arrayed in the transverse direction. Although the use of a DSA for the SKAMP line feed offers the possibility of meeting the impedance and scanning bandwidth requirements over the operating frequency, its applicability is limited by the high engineering complexity and cost.

Sinuous antennas have a wideband pattern bandwidth, but its scanning bandwidth does not cover the SKAMP operating frequency. The relatively large element size limits the scanning bandwidth. Advantages of this element are its wideband radiation pattern performance and planar construction. The impedance bandwidth can be extended to 11:1, providing a –6 dB return loss is acceptable. A sinuous antenna has been used in a parabolic reflector described in Section 4.1.5. However, its element size of 0.5λ at the lower frequency limits its ability to scan to large angles without the appearance of grating

lobes. This is not usually a problem in parabolic reflectors because the beam must be captured by the reflector to avoid spillover and defocusing from the reflector curvature.

Although the densely spaced array antenna meets the SKAMP impedance and scanning bandwidth specifications, the engineering complexity and costs are high. On the other hand, the wideband dipole, wideband patch and sinuous antennas have more realistic engineering requirements for SKAMP. However, their impedance and scanning bandwidth does not cover the entire SKAMP bandwidth. Sinuous antennas have modest engineering complexity, but their large size would restrict their scanning performance and compromise the survey sensitivity. On balance, the best options from Table 4.1 for the SKAMP line feed design are the wideband dipole and wideband patch elements. Comparing these two elements; the wideband dipole has better polarisation performance, lower back radiation and simpler engineering requirements for the SKAMP frequency range. However, to cover the entire SKAMP operating frequency range multiple line feeds are required.

4.3 Line Feed Solution

A line feed scanning bandwidth of more than 2:1 is difficult to achieve for a scan angle range of ±60°, due to grating lobes, resonances, increased mutual coupling and polarisation and pattern degradation at large scan angles. For example, a densely spaced array using TSA elements with a 5:1 scan impedance bandwidth for a ±50° scan range reduces to a 1.6:1 bandwidth for a ±60° scan range, satisfying a return loss < –10 dB (Holter 2001). From Table 4.1, the wideband dipole line feed has a 1.5:1 scanning bandwidth across the whole ±60° scan range. Multiple line feeds are necessary for operation across the entire SKAMP 4.7:1 observing bandwidth. This approach is reasonable, providing each line feed has an instantaneous bandwidth of at least 100 MHz. Table 4.2 describes a possible three-band line feed solution, each with a bandwidth of around 1.7:1, to cover the full frequency range.

Band (MHz)	Centre Frequency (MHz)
300–500	400
500–840	670
840–1400	1120

Table 4.2 Three line feed bands covering 300–1400 MHz.

A three-band solution has some weaknesses. For an element size of $0.35\lambda_L$ and a bandwidth of 1.7:1, the scan angle range before a grating lobe appears in the field-of-view is ±45°, as calculated by Equation 3.12. This can be extended to ±60° by reducing the element size to $0.32\lambda_L$. A characteristic of phased arrays is that the gain is reduced when electrically scanned because of aperture foreshortening. This foreshortening at large scan angles will reduce the received power and survey sensitivity, and limits the negative effect of the grating lobe on performance, as described in Section 3.3.2. The gain reduction for the current MOST operation can be determined from the MD gain curve (EWGF) in Figure 2.6. For a scan angle of ±45°, the reduction is 50%. In addition, other parameters could limit the scanning performance at large scan angles, so the maximum scan angle range may not be limited by the element size. These parameters include: polarisation, impedance, back radiation and resonances due to the element

construction and geometry. An investigation into the performance of the wideband dipole with scan angle is presented in Chapter 7.

The design approach, to achieve the three-band line feed solution is to firstly develop a single band with a bandwidth of 1.7:1. Its performance will be characterised across its bandwidth and scan angle range. Optimisation techniques are applied to improve any line feed limitations that cannot be easily corrected through calibration. When the design has been characterised, its dimensions are then scaled appropriately to obtain the other bands. The initial frequency band selected for the design is around 500–1000 MHz, which will allow major scientific objectives to be met. The centre frequency is taken as the geometric mean of the frequency band, 866 MHz. The design frequency range also enables compatibility with existing electronics and infrastructure at the MOST operating frequency, 843 MHz.

The three-band line feed solution will be mounted in the focal region at the MOST. If the line feed mounting configuration is not in the focal region, defocusing effects occur which increase the noise temperature. A reflector focal region analysis is required to determine the distance a line feed can be displaced before defocusing effects occur. Two possible configurations to mount the multiple feeds are a contiguous arrangement using feeds aligned in the transverse plane and a rotating triangular-shaped turret with the feeds placed on each face. These configurations are shown respectively in Figures 4.19(a) and 4.19(b). From an engineering viewpoint, the contiguous mount is preferable because no mechanical moving parts are required to change operating bands. However, from an electrical viewpoint, the turret has less aperture blockage and better aperture efficiency.

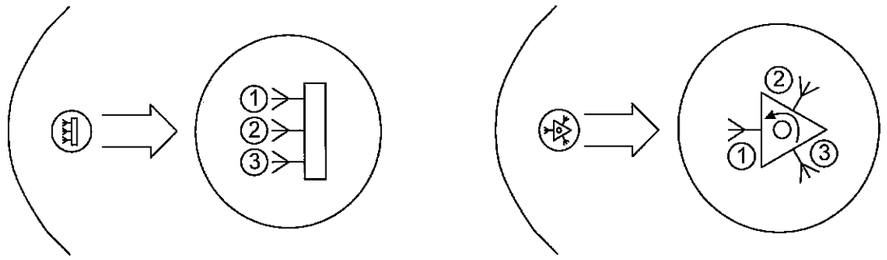

Figure 4.19 Two possible feed configurations for SKAMP, with numbers indicating the three line feed bands (a) Contiguous configuration. (b) Rotating turret configuration.

4.4 Summary

A literature survey of the current state-of-the-art in phased array antenna element technology was reviewed. This was required to determine a suitable antenna technology for the line feed design investigated in this thesis. The selection of the particular element for the SKAMP line feed is based on criteria established in Section 3.3. Although the densely spaced array element is the ideal line feed element from an impedance and scanning bandwidth viewpoint, it is difficult to implement at the MOST. This is due to the large number of elements required to feed the reflector and increased design complexity of the subsequent feed network, electronics and signal processing systems. A wideband dipole element was selected as the most suitable feed element for the SKAMP

300–1400 MHz frequency range, because of its ease of manufacture, good polarisation and low back radiation performance. Hybrid couplers were used to feed several wideband dipoles described in Section 4.1.2. This feeding technique is undesirable, as it introduces additional loss and cost. A low cost, low loss, wideband dual polarised balun is investigated in Chapter 7. Because the scanning bandwidth of the selected element is only 1.5:1 and a multiple line feed solution is outlined in Section 4.3 to cover the entire operating frequency range. A three-band line feed solution was proposed, with each line feed consisting of a bandwidth of 1.7:1. Two mounting configurations for the three-band solution presented in Section 4.3 were: feeds positioned contiguously and on a triangular rotating turret.

The initial design frequency range for the feed prototype was selected as 500–1000 MHz, allowing major science objectives to be met. After this design has been evaluated, it can then be scaled appropriately to form the additional two-bands required to cover the entire operating frequency range. The SKAMP line feed transverse half-power beamwidth range is a parameter that remains unspecified. This parameter determines reflector pattern characteristics such as aperture efficiency, sidelobe levels and spillover temperature. Both the HPBW specification and selection of the mounting configuration are dependent on the performance of the line feed in the cylindrical reflector. The current model used to determine the reflector pattern as described in Section 2.5 does not accurately represent the HPBW at large scan angles. A model for the reflector pattern to determine the feed transverse HPBW range and size of the focal region for the line feed mounting configuration is presented in Chapter 5.